

Supporting Information for

**Ferrate(VI) oxidation of  $\beta$ -lactam antibiotics: reaction kinetics,  
antibacterial activity changes, and transformation products**

Anggita Karlesa<sup>1</sup>, Glen Andrew D. De Vera<sup>1,2</sup>, Michael C. Dodd<sup>3</sup>, Jihye Park<sup>1</sup>,  
Maria Pythias B. Espino<sup>2</sup>, and Yunho Lee<sup>1\*</sup>

<sup>1</sup>Department of Environmental Science and Engineering, Gwangju Institute of Science and  
Technology (GIST), Gwangju 500-712, Republic of Korea

<sup>2</sup>Institute of Chemistry, College of Science, University of the Philippines, Diliman, Quezon City  
1101, Philippines

<sup>3</sup>Department of Civil and Environmental Engineering, University of Washington, Seattle, WA  
98195, USA

**This PDF file includes:**

9 texts, 3 tables, 21 figures, and 3 schemes addressing materials, experimental procedures, and  
additional data

## SI-Text-1. Standards and reagents

Potassium ferrate was purchased from Sigma-Aldrich ( $K_2FeO_4$ , 723835). The purity of this product was ~82 % as Fe(VI) (w/w) which was determined by dissolving known amounts of solid samples in phosphate buffer solutions (5 mM  $Na_2HPO_4$ / 1 mM borate, pH  $\approx$  9.2), subsequent filtration through a 0.45  $\mu$ m PVDF syringe filters (Whatman, USA), and measuring the Fe(VI) concentration by both the direct 510 nm method ( $\epsilon = 1150 \text{ M}^{-1} \text{ cm}^{-1}$ )<sup>1</sup> and the ABTS method<sup>2</sup>. Stock solutions of Fe(VI) (0.2–3 mM) were freshly prepared by dissolving solid samples of potassium ferrate in pure water (pH  $\approx$  9.2). The fresh stock solution was also quickly filtered through a 0.45  $\mu$ m PVDF syringe filter (Whatman, USA) and then standardized spectrophotometrically at 510 nm<sup>1</sup>. Ozone stock solutions (1 – 1.5 mM) were prepared by sparging ozone-containing oxygen through deionized water that was cooled in an ice bath and were standardized spectrophotometrically based on the molar absorption coefficient,  $\epsilon = 3000 \text{ M}^{-1} \text{ cm}^{-1}$  at 258 nm<sup>3</sup>. An ozone generator from Ozone Tech (Ozone generator LAB-1 model, Korea, <http://www.ozonetech.co.kr/>) was used.

2-amino-2-phenyl-acetamide (APA, 533157), 3,5-dimethylisoxazole (DMIZ, D167509), amoxicillin (AMX, A8523), ampicillin (AMP, A6140), cephalexin (CEX, C4895), cloxacillin (CLOX, C9393), and Penicillin G (PENG, 13752) were purchased from Sigma-Aldrich. 3-methylcrotonic acid (MCA, M0543) was purchased from Tokyo Chemical Industry Co., Ltd. Stock solutions of  $\beta$ -lactam antibiotics and model compounds were prepared in ultrapure water at concentrations of 0.1 – 2 mM.

The following chemicals were commercially available and used for pH buffers, acids, bases, and solvents: phosphoric acid (85%  $H_3PO_4$  in  $H_2O$ , Sigma-Aldrich, W290017), sodium phosphate monobasic ( $NaH_2PO_4 \cdot 2H_2O$ , Sigma-Aldrich, 71500), sodium phosphate dibasic ( $Na_2HPO_4 \cdot 2H_2O$ , Sigma-Aldrich, 30412), sodium tetraborate ( $NaB_4O_7$ , Sigma-Aldrich, 31457), sulfuric acid (Sigma-Aldrich, 320501), sodium hydroxide (50% NaOH in  $H_2O$ , Sigma-Aldrich), acetonitrile (Fisher Scientific, A998-4), and methanol (Fisher Scientific, A452-4). 2,2'-Azino-bis(3-ethylbenzothiazoline-6-sulfonic acid) diammonium salt (ABTS, 11557) was purchased from Sigma-Aldrich.

## SI-Text-2. Determination of reaction order and rate constants

Kinetic studies of Fe(VI) reactions were performed in the pH range 6 – 10. For all pH conditions, phosphate (5 – 10 mM) was used as a buffer as well as a complexing agent for Fe(III). Formation of the soluble Fe(III)-phosphate complexes prevents the precipitation of Fe(III) which might interfere with the optical monitoring of the ferrate(VI) reaction solutions<sup>1,2</sup>. Together with the phosphate buffer, borate (2 – 5 mM) was used as a buffer for the pH range 8.5–9.5. Phosphate and borate are expected to react very slowly with Fe(VI) ( $k \ll 0.1 \text{ M}^{-1} \text{ s}^{-1}$ )<sup>4</sup>, and therefore would not interfere with the Fe(VI) reactions of interest under the experimental conditions of this study. The kinetic experiments using the organic compound in excess method were performed in a water bath at  $25 \pm 1^\circ\text{C}$ , and the kinetic experiments using the Fe(VI) in excess method at room temperature of  $21 \pm 2^\circ\text{C}$ .

*Organic compound in excess method.* Kinetic experiments were conducted under pseudo-first order conditions with the target compound (i.e.,  $\beta$ -lactams and model compounds) in excess of Fe(VI) ( $[\text{compound}]_0 > 10 \times [\text{Fe(VI)}]_0$  and  $[\text{Fe(VI)}]_0 = 1 - 3 \text{ }\mu\text{M}$ ). The reaction was initiated by adding a small volume ( $< 2 \text{ mL}$ ) of an aliquot of Fe(VI) stock solution ( $0.1 - 0.3 \text{ mM}$ ) to a thermostated solution ( $200 \text{ mL}$ ) containing a given  $\beta$ -lactam or model compound and buffered at a desired pH under rapid mixing. The reaction solutions were then sampled as a function of reaction time (typically within 10 min) and quenched with an ABTS solution to measure residual Fe(VI) concentrations<sup>2</sup>. The Fe(VI) self-decay was found to be less than 5% in all experimental conditions due to the low applied initial Fe(VI) concentration (i.e.,  $1 - 3 \text{ }\mu\text{M}$ )<sup>4,5</sup>. For all investigated compounds, Fe(VI) followed a pseudo-first order decrease, confirming that the reaction is first-order with respect to Fe(VI). The pseudo-first order rate constants ( $k_{\text{pseudo-first}}$ ) were calculated from the slope of the linear curve resulting from plots of natural logarithmic relative concentration of Fe(VI) versus reaction time. Figure S1 shows an example for cephalexin (CEX).

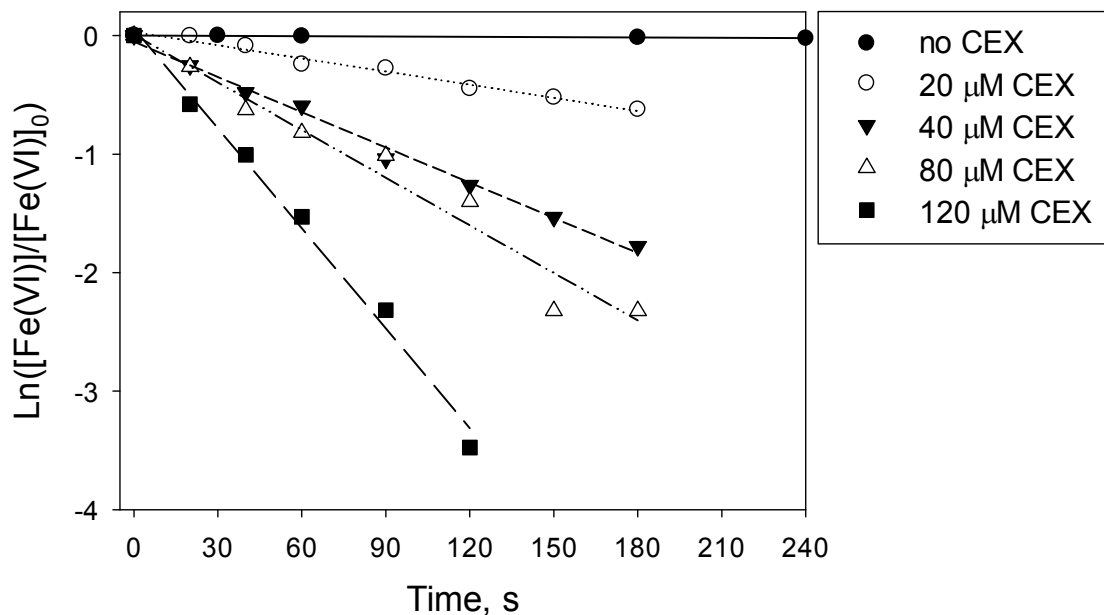


Figure S1. Logarithmic relative concentration of Fe(VI) as a function of reaction time during the reaction of 2  $\mu\text{M}$  of Fe(VI) with an excess of cephalixin (CEX) ( $[\text{CEX}]_0 = 0, 20, 40, 80, \text{ and } 120 \mu\text{M}$ ) at pH 8. Symbols represent the measured data and lines represent the linear regressions.

The  $k_{\text{pseudo-first}}$  values were determined at various concentrations of compounds. For all investigated compounds,  $k_{\text{pseudo-first}}$  increased linearly with increasing concentration of compounds. Figure S2 shows that the slope of a plot of  $\log(k_{\text{pseudo-first}})$  vs  $\log([\text{CEX}])$  is close to unity indicating that the reaction is first-order with respect to CEX concentration. Apparent second-order rate constants ( $k_{\text{app}}$ ) were then obtained by dividing the pseudo first-order rate constants ( $k_{\text{pseudo-first}}$ ) by the concentration of the compound. The compound in excess method was applied to PENG, CLOX, AMP, AMX, CEX, APA, MCA, and DMIZ and the kinetic results are shown Table S1 (see also Figure 1).

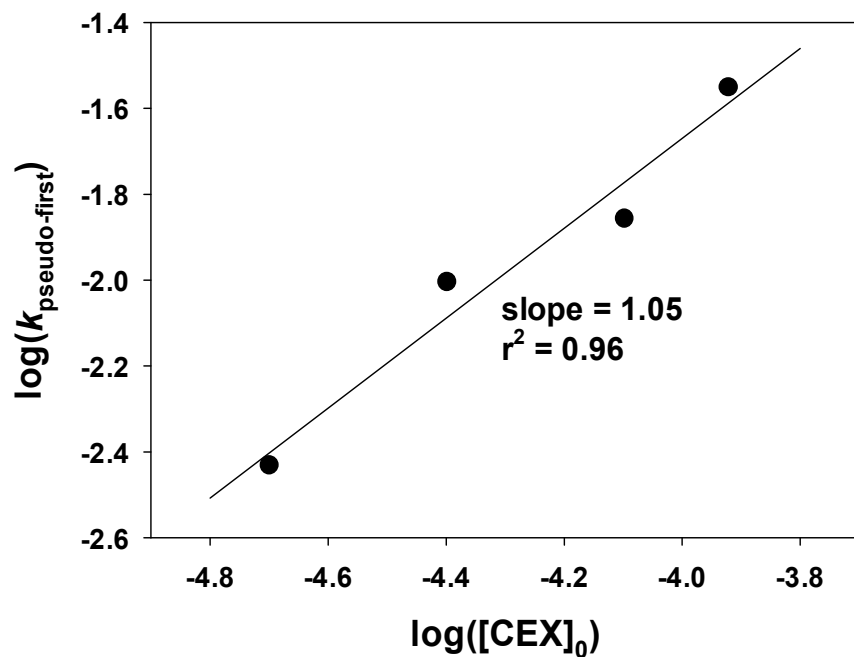
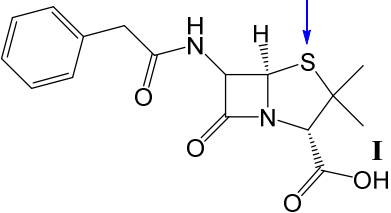
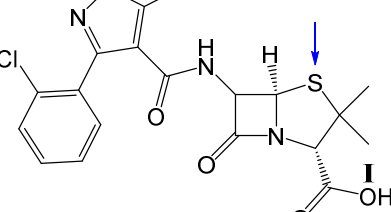
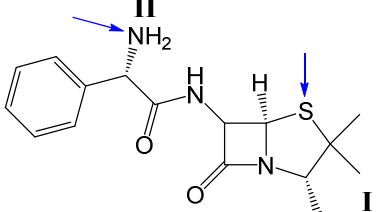
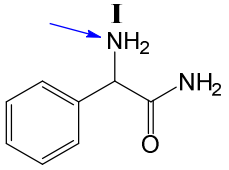
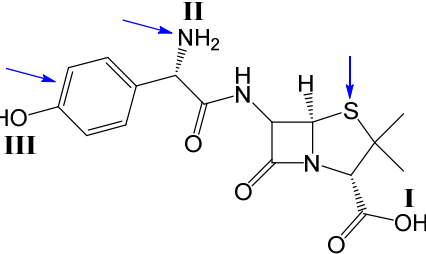


Figure S2. Logarithmic plot of the pseudo-first-order rate constant for the decrease of Fe(VI) ( $k_{\text{pseudo-first}}$ ) vs. the initial CEX concentration at pH 8. The symbols represent the experimental data,, while the line represents a linear fit of the data with slope as indicated.

96 Table S1. Structures of target  $\beta$ -lactam antibiotics and their substructure model compounds, and  
 97 the second-order reaction rate constants with Fe(VI)

Compounds <sup>a</sup>	$k$ (species-specific), $M^{-1} s^{-1}$	$k_{app-pH}$ , $M^{-1} s^{-1}$
 <p>Penicillin G (PENG),  <math>pK_{a,I} = 2.8^b</math></p>	$k_{HFeO_4^-/S} = 1.8(\pm 0.2) \times 10^2$ $k_{FeO_4^{2-}/S} = 9.7(\pm 1.8)$	$k_{app-pH-7} = 114$ $k_{app-pH-8.5} = 18$
 <p>Cloxacillin (CLOX),  <math>pK_{a,I} = 2.7^b</math></p>	$k_{HFeO_4^-/S} = 1.8(\pm 0.3) \times 10^2$ $k_{FeO_4^{2-}/S} = 15.4(\pm 4.1)$	$k_{app-pH-7} = 116$ $k_{app-pH-8.5} = 24$
 <p>Ampicillin (AMP),  <math>pK_{a,I} = 2.7^b</math>, <math>pK_{a,II} = 6.4(\pm 0.5)^c</math> or = <math>6.7^d</math></p>	$k_{HFeO_4^-/NH_2} = 6.2(\pm 2.0) \times 10^2$ $k_{HFeO_4^-/S} = 1.8 \times 10^2$ $k_{FeO_4^{2-}/S} = 12.6$	$k_{app-pH-7} = 418$ $k_{app-pH-8.5} = 50$
 <p>2-amino-2-phenylacetamide (APA)  <math>pK_{a,I} = 6.7(\pm 0.2)^c</math> or = <math>7.2^d</math></p>	$k_{HFeO_4^-/NH_2} = 7.1(\pm 1.2) \times 10^2$	$k_{app-pH-7} = 285$ $k_{app-pH-8.5} = 34$
 <p>Amoxicillin (AMX),  <math>pK_{a,I} = 2.4^b</math>, <math>pK_{a,II} = 6.7(\pm 0.2)^c</math> or = <math>6.9^d</math>, <math>pK_{a,III} = 9.6^b</math></p>	$k_{HFeO_4^-/NH_2} = 1.4(\pm 0.5) \times 10^3$ $k_{HFeO_4^-/PhO^-} = 2.1 \times 10^4$ $k_{HFeO_4^-/PhOH} = 1.0 \times 10^2$ $k_{HFeO_4^-/S} = 1.8 \times 10^2$ $k_{FeO_4^{2-}/S} = 12.6$	$k_{app-pH-7} = 771$ $k_{app-pH-8.5} = 162$

 Cephalexin (CEX), $pK_{a,I} = 5.3^b$ , $pK_{a,II} = 6.4^c$ or $6.6^d$	$k_{HFeO_4^-/NH_2} = 6.2 \times 10^2$ $k_{HFeO_4^-/S} = 6.1(\pm 2.0) \times 10^2$ $k_{FeO_4^{2-}/S} = 16.4(\pm 8.7)$	$k_{app-pH-7} = 686$ $k_{app-pH-8.5} = 74$
 3-methylcrotonic acid (MCA) $pK_{a,I} = 5.2$	$k_{HFeO_4^-/olefin} = 3.5(\pm 0.5)$ $k_{FeO_4^{2-}/olefin} = 0.4(\pm 0.1)$	$k_{app-pH-7} = 2.3$ $k_{app-pH-8.5} = 0.5$
 3,5-dimethylisoxazole (DMIZ)		$k_{app-pH-8} = 0.17(\pm 0.01)$

<sup>a</sup>The arrows indicate the expected main reaction site during Fe(VI) oxidation, <sup>b</sup>from ref. 6, <sup>c</sup>best-fitting  $pK_a$  values for the kinetic data (see the main text), <sup>d</sup>predicted by SPARC (<https://archemcalc.com>).

*Fe(VI) in excess method.* Kinetic experiments were also conducted under pseudo-first-order conditions with Fe(VI) in excess of the  $\beta$ -lactam antibiotics (i.e.,  $[Fe(VI)]_0 > 10 \times [\beta\text{-lactam}]_0$ , and  $[\beta\text{-lactam}]_0 = 1 - 2 \mu\text{M}$ ) and the decrease of the  $\beta$ -lactam and Fe(VI) concentrations were measured as a function of the reaction time. The kinetic runs were started by adding an aliquot of a Fe(VI) stock solution (1 – 2 mM) to a solution (200 mL) containing a given  $\beta$ -lactam and buffered at a desired pH under rapid mixing. At proper time intervals, 1–5 mL of the reaction solution were sampled and quenched with a thiosulfate solution (5 mM) to measure residual  $\beta$ -lactam antibiotic concentrations as well as with an ABTS solution to measure residual Fe(VI) concentrations. It was necessary to measure the rate of Fe(VI) decrease because Fe(VI) decomposed more than 10% via self-decomposition at initial Fe(VI) concentrations of  $>10 \mu\text{M}$  and at  $pH < 9^{4,5}$ . The data was evaluated by plotting the natural logarithm of the relative  $\beta$ -lactam concentration vs. the Fe(VI) exposure, i.e., Fe(VI) concentration integrated over time, as shown in eq 1:

$$-\ln\left(\frac{[\beta\text{-lactam}]}{[\beta\text{-lactam}]_0}\right) = k'_{app} \int [Fe(VI)] dt \quad (1)$$

where the  $\int [Fe(VI)] dt$  term represents the Fe(VI) exposure – the time integrated concentration of Fe(VI), and  $k'_{app}$  (the slope of the resulting straight line) represents the apparent second-order rate

constant. The  $k'_{app}$  differs from the  $k_{app}$  (that is determined by the compound in excess method) by a reaction stoichiometry factor ( $\eta$ ), where  $k_{app} = \eta k'_{app}$ .

Figure S3 shows the concentration time profiles of cephalexin (CEX) and Fe(VI) during the oxidation of CEX (2  $\mu$ M) by excess Fe(VI) (40  $\mu$ M) at pH 6.5 as representative data. Even though Fe(VI) was unstable, the Fe(VI) concentration was always in excess of the CEX concentration within the studied reaction time. Figure S3 clearly shows that eq 1 successfully represents the kinetics of CEX transformation by Fe(VI) oxidation ( $R^2 = 0.99$ ). From the slope of the line in Figure S3b, the  $k'_{app}$  was determined as  $k'_{app} = 18.7 \text{ M}^{-1} \text{ s}^{-1}$  at pH 6.5. The Fe(VI) in excess method was applied to PENG, CLOX, AMX, and CEX and the kinetic results are shown in Figure 1.

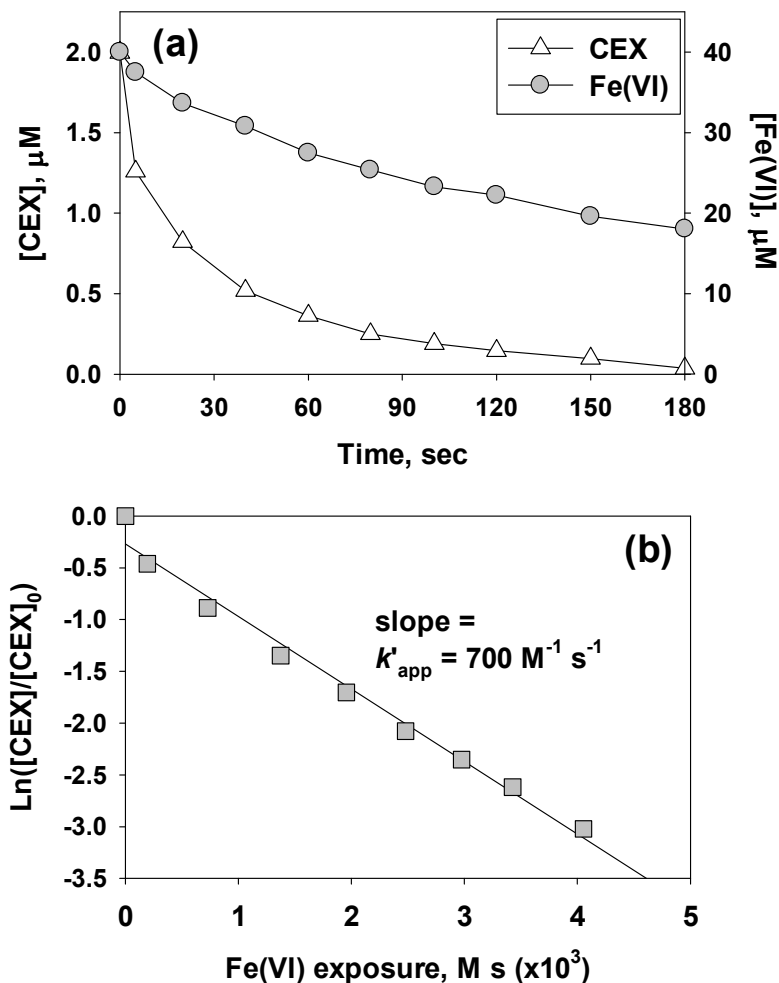


Figure S3. (a) Decrease of CEX and Fe(VI) as a function of time during the reaction of 2  $\mu$ M of CEX with 40  $\mu$ M of Fe(VI) at pH 6.5, and (b) fit of CEX transformation by Fe(VI) with second-



order reaction kinetics (i.e., eq 1). The slope of the linear fit represents the apparent second-order rate constant ( $k'_{app}$ ) for the reaction of CEX with Fe(VI) at pH 6.5.

### **SI-Text-3. HPLC/UV method for $\beta$ -lactam analysis**

$\beta$ -lactams were analyzed with a HPLC system equipped with a UV diode array detector (Ultimate 3000, Dionex). Separation was achieved by an Acclaim 120 C18 column (5  $\mu$ m, 4.6 $\times$ 250mm, Dionex) using an aqueous phase consisting of 10 mM phosphoric acid and an organic solvent phase of either acetonitrile or methanol. The injection volume was 100  $\mu$ L and the flow rate was set to 1 mL min<sup>-1</sup> (Acclaim column). The repeatability was determined to be 4% while limits of quantification (LOQ) were inferred from the lowest standard concentrations used. The limits of quantification were  $\sim$ 0.05  $\mu$ M for all  $\beta$ -lactams.

### **SI-Text-4. Elimination of $\beta$ -lactams by Fe(VI) in a wastewater effluent**

A wastewater effluent sample was collected as a grab sample (5 L) from the Gwangju wastewater treatment plant (GJWW), Korea. This plant has a 600,000 m<sup>3</sup> day<sup>-1</sup> operation capacity and uses an activated sludge system equipped with a primary clarifier, nitrification, denitrification, and chlorine disinfection before discharge. The sample was collected from the secondary biological treatment effluent and before the chlorination. The effluent was vacuum-filtered by glass membrane filter (GF/F, 47mm, Whatman, USA) upon arrival to laboratory and stored at 4°C until use. The water quality parameters of the effluent are as follows: DOC = 7.3 mgC/L, pH =  $\sim$ 7, alkalinity = 1.7 mM as HCO<sub>3</sub><sup>-1</sup>, TN = 8.9 mgN/L, NH<sub>4</sub><sup>+</sup> = 0.5 mgN/L, NO<sub>2</sub><sup>-</sup> = 0.08 mgN/L, NO<sub>3</sub><sup>-</sup> = 6.7 mgN/L, and PO<sub>4</sub>-P = 0.9 mgP/L respectively. TOC and TN were analysed by TOC-V<sub>CPH</sub> Total Organic Carbon analyzer connected to a TNM-1 Total Nitrogen measuring unit (Shimadzu, Japan). Alkalinity was determined through acidic-titration using a pH of 4.2 as a titration end-point. Anions was analysed by a Dionex ICS-90 Ion Chromatography System equipped with an Ion Pac AS14 column (4 mm x 250 mm) and Ion Pac AG 14 guard column (4 mm x 50 mm). NH<sub>3</sub>-N was measured with the Nessler method (Hach Method 8038).

The wastewater effluent sample was buffered by adding 20 mM bicarbonate buffer for pH 7 or 10 mM borate buffer for pH 8.5. These two pH values were selected to cover the typical pH range of municipal wastewaters. The sample was then spiked with each  $\beta$ -lactam at 2  $\mu$ M. As typical

background concentrations of organic micropollutants including  $\beta$ -lactams in municipal wastewater effluents are sub to a few  $\mu\text{g/L}$  range ( $\ll 2 \mu\text{M}$ ), the overall initial  $\beta$ -lactam concentration for Fe(VI) oxidation experiments (including background) was  $2 \mu\text{M}$ .

To assess the competition for Fe(VI) between the wastewater matrix and the  $\beta$ -lactams, the wastewater effluent spiked with each  $\beta$ -lactam was treated by Fe(VI) with doses of 0.7, 1.8, 3.7, and  $5.5 \text{ mgFe/L}$  (i.e.,  $[\text{Fe(VI)}]_0/[\text{DOC}] = 0.1, 0.25, 0.5,$  and  $0.75$  as  $\text{gFe/gC}$ , respectively). After 1 h, residual concentrations of  $\beta$ -lactam were measured by the HPLC/UV method after filtering the samples through  $0.45 \mu\text{m}$  PVDF syringe filters (Whatman, USA) to remove iron-precipitates. Losses of  $\beta$ -lactams during the filtration were negligible. Fe(VI) decrease was also measured in GJWW as a function of the reaction time with the ABTS method<sup>2</sup>. Figures S4 and S5 show the measured Fe(VI) decrease in GJWW at various initial Fe(VI) doses at pH 7 and pH 8.5, respectively. Fe(VI) exposures (i.e., time-integrated Fe(VI) concentration), were calculated from the areas below the Fe(VI) decay curves. Figure S6 shows the determined Fe(VI) exposures as a function of Fe(VI) dose in GJWW at pH 7 and 8.5.

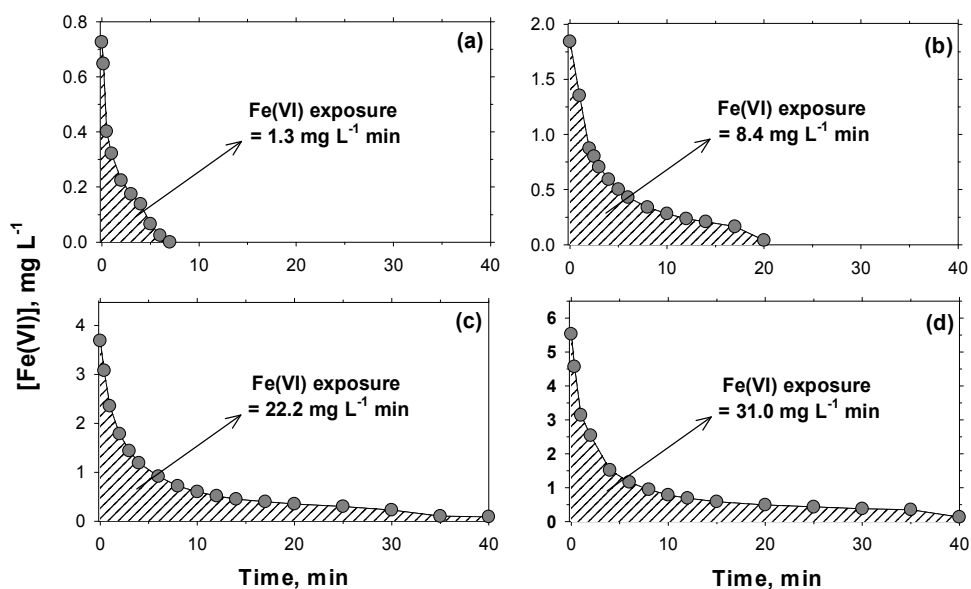


**Figure S4.** Decrease of Fe(VI) in Gwangju wastewater effluent at pH 7 (20 mM bicarbonate buffer). Experimental conditions: Initial Fe(VI) dose = (a) 0.7, (b) 1.8, (c) 3.7, and (d)  $5.5 \text{ mgFe L}^{-1}$ .

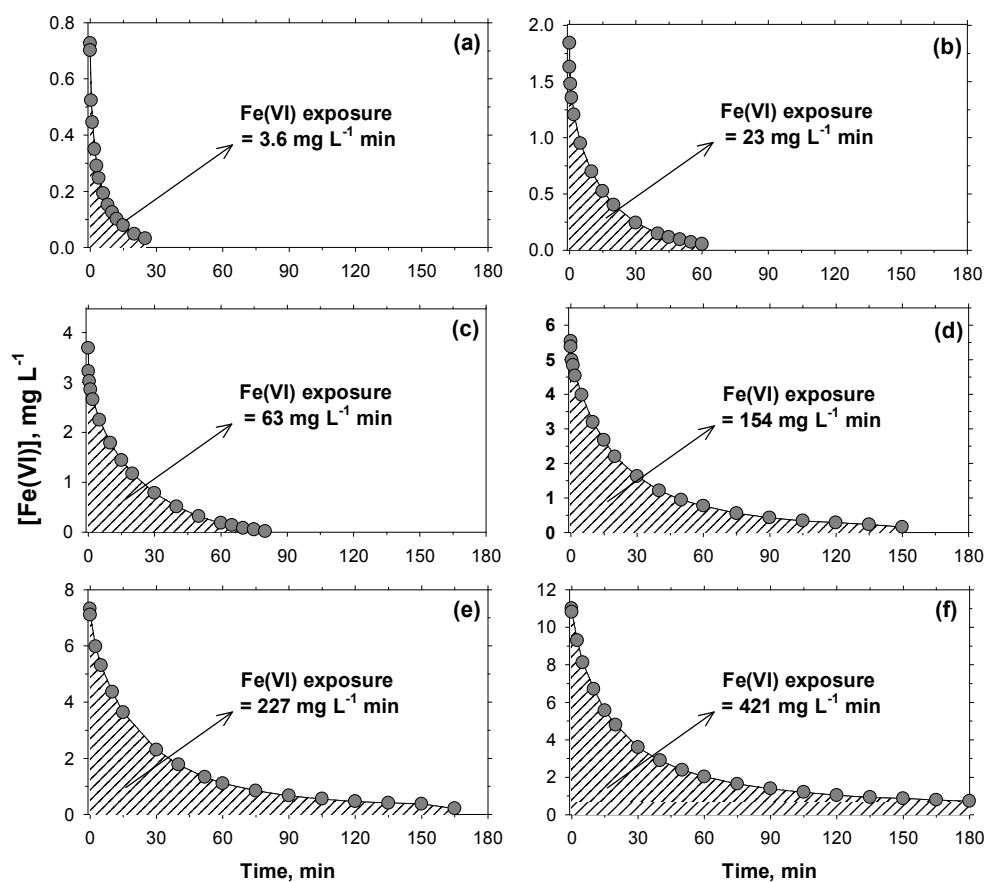


**Figure S5.** Decrease of Fe(VI) in Gwangju wastewater effluent at pH 8.5 (10 mM borate buffer). Experimental conditions: Initial Fe(VI) dose = (a) 0.7, (b) 1.8, (c) 3.7, (d) 5.5, (e) 7.3, and (f) 11.0 mgFe L<sup>-1</sup>.

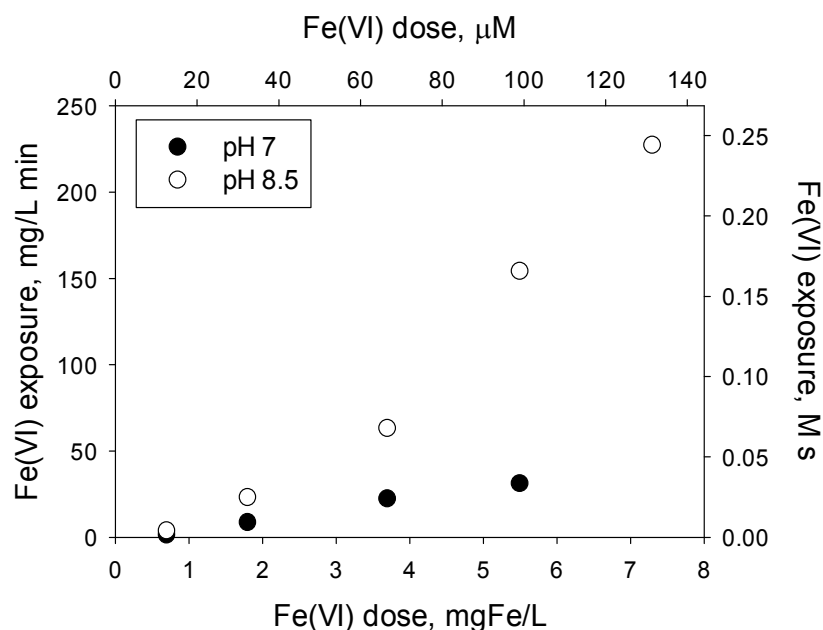


**Figure S6.** Fe(VI) exposures in a wastewater effluent (GJWW) as a function of Fe(VI) dose.

#### SI-Text-5. Comparison of Fe(VI) reactivity toward thioether moieties.

Second-order rate constants for the reaction of Fe(VI) with thioethers have been reported for methionine ( $k = 8.2 \times 10^3 \text{ M}^{-1} \text{ s}^{-1}$ )<sup>7</sup>, ethionine ( $k = 5.7 \times 10^3 \text{ M}^{-1} \text{ s}^{-1}$ )<sup>8</sup>, and thioxane ( $k = 2.5 \times 10^3 \text{ M}^{-1} \text{ s}^{-1}$ )<sup>9</sup>. These rate constants are 14–45 times of the rate constant for the thioether of penicillins ( $k = 1.8 \times 10^2 \text{ M}^{-1} \text{ s}^{-1}$ , Table S1) or 4–12 times of that of cephalexin ( $k = 6.9 \times 10^2 \text{ M}^{-1} \text{ s}^{-1}$ , Table S1). Steric hindrance might be responsible for the different reactivity of Fe(VI) to these compounds. The sulfur of thioxane, a six-membered ring compound, is more sterically hindered compared to methionine or ethionine in which the sulfur is connected to non-ring aliphatic carbons. This explains the 2–3 fold lower reactivity of thioxane compared to methionine and ethionine. Similarly, the lower reactivity of the sulfur atom in  $\beta$ -lactams may be attributable to steric hindrance arising from its fusion to the neighboring  $\beta$ -lactam ring. Finally, the observed larger reactivity of cephalexin could be explained by decreased steric hindrance toward reaction of Fe(VI) with the thioether in the six-membered ring system – which lacks an adjacent dimethyl group – compared to the thioether in the five-membered ring systems of the penicillins.

To confirm the observed higher reactivity of CEX's thioether moiety compared to that of the penicillins, 100  $\mu\text{M}$  of CEX was pre-treated with an equal concentration of chlorine at pH 3 to transform the thioether moiety selectively (but not the amine). Note that the amine moiety of CEX

is completely protonated at pH 3 and reacts very slowly with chlorine<sup>10</sup>, while the thioether's reactivity remains high. No chlorine residual was found right after the chlorine reaction, indicating that the added chlorine was rapidly and completely consumed by the thioether moiety of CEX. Decrease of Fe(VI) was measured in the chlorine-treated sample after re-adjusting the sample pH from 3 to 7. This yielded a  $k_{\text{app}}$  value of  $330 \text{ M}^{-1} \text{ s}^{-1}$  – similar to the  $k_{\text{app}}$  value at pH 7 for AMP or APA, which each contain an amine moiety as a primary site of reaction with Fe(VI). This in turn indicates that the higher magnitude of  $k_{\text{app}}$  at pH 7 ( $= 686 \text{ M}^{-1} \text{ s}^{-1}$ ) for reaction of non-chlorine-treated CEX with Fe(VI) can be attributed to the intact CEX thioether moiety, consistent with its higher reactivity toward Fe(VI) compared to the thioether moiety of PENG, AMP, and AMX.

#### SI-Text-6. Comparison of $k_{\text{app}}$ for AMP and AMX with literature values.

Figure S7 compares the  $k_{\text{app}}$  data for AMP and AMX determined in this study with those reported in literature<sup>11</sup>. Despite the similar pH dependent variations in  $k_{\text{app}}$ , the literature  $k_{\text{app}}$  values were 2 – 4 times higher than those obtained in this study in the pH range of 6 – 9. The reason for the discrepancy is not clear.

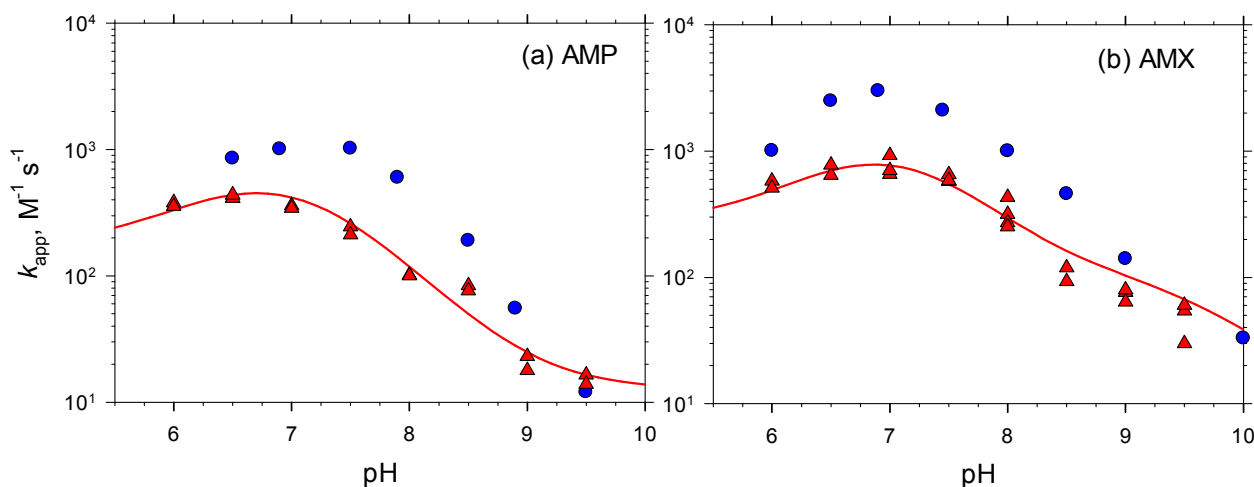
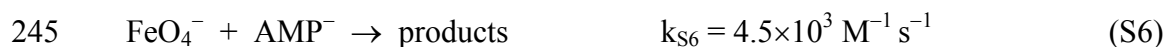


**Figure S7.** Comparison of  $k_{\text{app}}$  determined from this study (red triangles-measured and lines-predicted) with those reported in literature<sup>11</sup> (blue circles). (a) AMP and (b) AMX. The  $k_{\text{app}}$  values were taken from Fig.2a in ref. 11.

In the previous study<sup>11</sup>, the pH-dependent  $k_{\text{app}}$  data for AMX was fitted using the following reactions.



237 These rate constants (i.e.,  $k_{\text{S}2}$ ,  $k_{\text{S}3}$ , and  $k_{\text{S}4}$ ) cannot be directly compared with our species-specific  
 238 rate constants (Table S1) because they are still composite rate constants for the reaction of Fe(VI)  
 239 with a few moieties of AMX. For example,  $\text{H}_2\text{AMX}$  species in eq S2 contain the thioether and  
 240 protonated phenol moieties and  $\text{HAMX}^-$  species in eq S3 contain the thioether, protonated phenol,  
 241 and deprotonated amine moieties as the reaction sites. Similarly, the pH-dependent  $k_{\text{app}}$  data for  
 242 AMP was fitted using the below reactions S5, S6, and S7. However, these composite rate  
 243 constants can also not be directly compared to our species-specific rate constants.



247

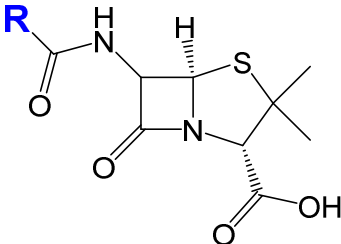
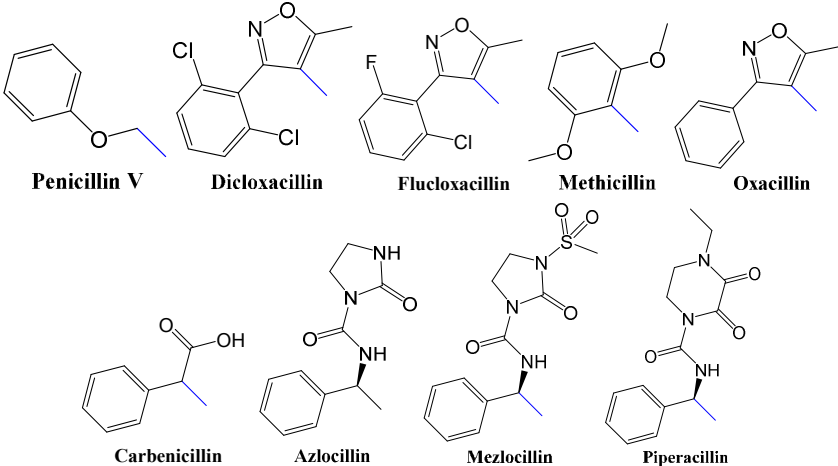
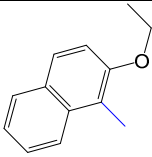
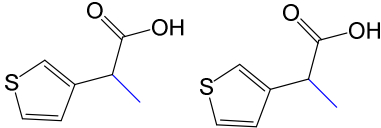
248

#### 249 **SI-Text-7. Prediction of $k_{\text{app}}$ for other penicillins and cephalosporins.**

250 The moiety-specific second-order rate constants determined in this study for the selected  
 251 penicillins and CEX (Table S1) can be used to predict the  $k_{\text{app}}$  of other structurally-related  
 252 penicillins (Table S2) and cephalosporins (Table S3). Table S2 shows that most penicillins (i.e.,  
 253 penicillin V, dicloxacillin, flucloxacillin, methicillin, oxacillin, carbenicillin, azlocillin, mezlocillin,  
 254 and piperacillin) contain the side chain (R, that is connected to the  $\beta$ -lactam ring by an amide bond)  
 255 which is much less reactive toward Fe(VI) than the thioether moiety. Thus, these penicillins are  
 256 expected to have the same reactivity as PENG or CLOX. Nafcillin contains a 2-ethoxy-  
 257 naphthalene moiety as the side chain which is expected to have a  $k_{\text{HFeO}_4^-}$  of  $18 \text{ M}^{-1} \text{ s}^{-1}$ . This  
 258 estimation is based on the  $k_{\text{HFeO}_4^-}$  of propranolol<sup>12</sup> in which the 1-alkoxy-naphthalene moiety is  
 259 one of the main reaction sites of Fe(VI). Due to the additional reaction site of 2-ethoxy-  
 260 naphthalene moiety, the  $k_{\text{app}}$  of nafcillin for pH 7 is slightly higher than that of PENG (i.e.,  $k_{\text{app-pH-}}$   
 261  $_{7.0} = 125 \text{ M}^{-1} \text{ s}^{-1}$  for nafcillin and  $= 114 \text{ M}^{-1} \text{ s}^{-1}$  for PENG, Table S2). Ticarcillin and temocillin  
 262 contain a thiophene moiety as the side chain in which the  $k$  value for their reaction with Fe(VI) is  
 263 currently unavailable. Considering the typical high reactivity of organic sulfur compounds toward  
 264 oxidants, the thiophene moiety is expected to have appreciable reactivity toward Fe(VI).

265

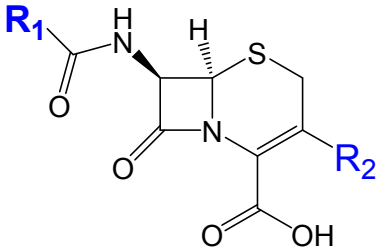
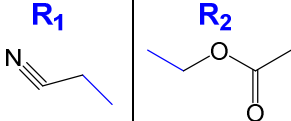
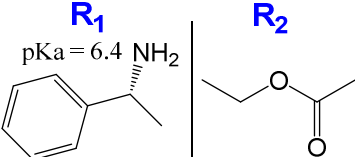
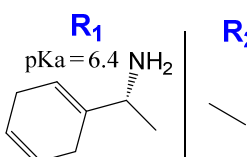
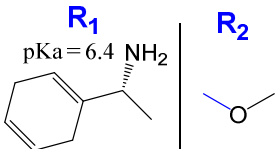
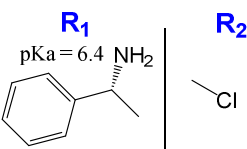
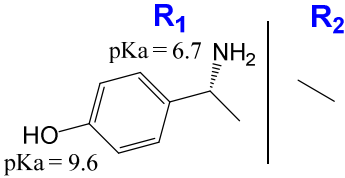
Table S2. Structures of penicillins and their predicted second-order reaction rate constants with Fe(VI)

 <b>Penicillins (R = side chain as shown below)</b>	<i>k</i> (species-specific), M <sup>-1</sup> s <sup>-1</sup>	<i>k</i> <sub>app-pH</sub> , M <sup>-1</sup> s <sup>-1</sup>
 Penicillin V    Dicloxacillin    Flucloxacillin    Methicillin    Oxacillin Carbenicillin    Azlocillin    Mezlocillin    Piperacillin	$k_{\text{HFeO}_4^-/\text{S}} = 177$ $k_{\text{FeO}_4^{2-}/\text{S}} = 13$	$k_{\text{app-pH-7.0}} = 114$ $k_{\text{app-pH-8.5}} = 21$
 Nafcillin methoxynaphthalene (MN)	$k_{\text{HFeO}_4^-/\text{S}} = 177$ $k_{\text{FeO}_4^{2-}/\text{S}} = 13$ $k_{\text{HFeO}_4^-/\text{MN}} = 18$	$k_{\text{app-pH-7.0}} = 125$ $k_{\text{app-pH-8.5}} = 22$
 Ticarcillin    Temocillin thiophene (TP)	$k_{\text{HFeO}_4^-/\text{S}} = 177$ $k_{\text{FeO}_4^{2-}/\text{S}} = 13$ $k_{\text{HFeO}_4^-/\text{TP}} = ?$	?

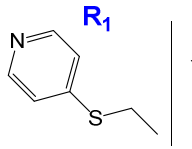
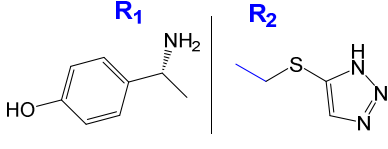
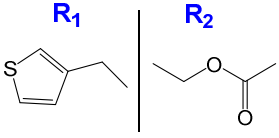
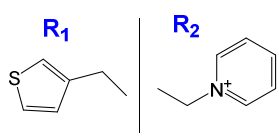
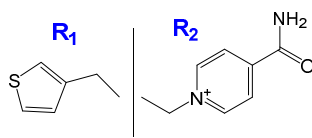
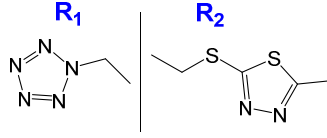
Cephalosporins contain two side chains and one of them (R<sub>1</sub>) is connected to the β-lactam ring by an amide bond and the other (R<sub>2</sub>) is directly connected to the six-membered ring (Table S3). The side chains of cefacetrile are expected to be non-reactive toward Fe(VI), thus the thioether moiety alone controls the overall reactivity for the reaction of cefacetrile with Fe(VI). Cefaloglycin, cefradin, cefroxadin, and cefaclor contain an amine moiety as the side chain 'R<sub>1</sub>'. Therefore, these cephalosporins will have the same reactivity as CEX. Cefadroxil contain the side

chain 'R<sub>1</sub>' with an amine and a phenol moiety whose reactivity toward Fe(VI) can be estimated from AMX that contains the same side chain. The *k*<sub>app</sub> of cefadroxil is larger than that of CEX due to the phenol as an additional reaction site and the increased reactivity of amine by the presence of hydroxyl group on the benzene in the side chain. Cefapirin, cefatrizine, cefalotin, cephaloridine, cefalonium, and cefazolin contain thiophene or aromatic thioethers in which the *k* value for their reaction with Fe(VI) is currently unavailable. Nevertheless, these organo sulfurs are expected to show an appreciable reactivity to Fe(VI). Overall, most cephalosporins are expected to show the same as or higher reactivity than CEX toward Fe(VI).

Table S3. Structures of cephalosporins and their predicted second-order reaction rate constants with Fe(VI)

 <p><b>Cephalosporins (R<sub>1</sub> and R<sub>2</sub> = side chains as shown below)</b></p>	<p><b><i>k</i> (species-specific), M<sup>-1</sup> s<sup>-1</sup></b></p>	<p><b><i>k</i><sub>app-pH</sub>, M<sup>-1</sup> s<sup>-1</sup></b></p>
 <p><b>Cefacetirle</b></p>	<p><i>k</i><sub>HFeO<sub>4</sub>-/S</sub> = 610 <i>k</i><sub>FeO<sub>4</sub>2-/S</sub> = 16</p>	<p><i>k</i><sub>app-pH-7.0</sub> = 380 <i>k</i><sub>app-pH-8.5</sub> = 44</p>
<div style="display: flex; justify-content: space-around;"> <div>  <p><b>Cefaloglycin</b></p> </div> <div>  <p><b>Cefradin</b></p> </div> </div> <div style="display: flex; justify-content: space-around;"> <div>  <p><b>Cefroxadin</b></p> </div> <div>  <p><b>Cefaclor</b></p> </div> </div>	<p><i>k</i><sub>HFeO<sub>4</sub>-/NH<sub>2</sub></sub> = 623 <i>k</i><sub>HFeO<sub>4</sub>-/S</sub> = 610 <i>k</i><sub>FeO<sub>4</sub>2-/S</sub> = 16</p>	<p><i>k</i><sub>app-pH-7.0</sub> = 686 <i>k</i><sub>app-pH-8.5</sub> = 74</p>
 <p><b>Cefadroxil</b></p>	<p><i>k</i><sub>HFeO<sub>4</sub>-/NH<sub>2</sub></sub> = 1380 <i>k</i><sub>HFeO<sub>4</sub>-/PhO-</sub> = 2100 <i>k</i><sub>FeO<sub>4</sub>2-/PhOH</sub> = 100 <i>k</i><sub>HFeO<sub>4</sub>-/S</sub> = 610 <i>k</i><sub>FeO<sub>4</sub>2-/S</sub> = 16</p>	<p><i>k</i><sub>app-pH-7.0</sub> = 1030 <i>k</i><sub>app-pH-8.5</sub> = 128</p>



 Cefapirin	 Cefatrizine		
 Cefalotin	 Cephaloridine	$k_{\text{HFeO}_4^-/\text{S}} = 610$ $k_{\text{FeO}_4^{2-}/\text{S}} = 16$ $k_{\text{HFeO}_4^-/\text{AT}} = ?$	?
 Cefalonium	 Cefazolin		
Aromatic thioethers (AT)			

## SI-Text-8. Identification of transformation products by HPLC/MS analysis

20  $\mu\text{M}$  of PENG or CEX were prepared in phosphate buffered solutions (1 mM) at pH 7 and treated with a range of Fe(VI) doses (10 – 120  $\mu\text{M}$ ). Parallel sets of such samples were also treated with ozone (10 – 60  $\mu\text{M}$ ) in the presence of *tert*-butanol (10 mM) as a  $\cdot\text{OH}$  radical scavenger. As the transformation products from the reactions of PENG and CEX with ozone were clearly identified previously<sup>13</sup>, the ozone-treated samples served as a benchmark for products comparison with Fe(VI)-treated samples. The reaction mixtures were left for 3 h to allow completion of each oxidation reaction. The Fe(VI) treated-samples were filtered through 0.45  $\mu\text{m}$  PVDF filters prior to analysis. Both the Fe(VI)- and ozone-treated samples were kept at 4°C until analysis.

Product mass analyses were performed using a HPLC (Alliance 2695, Waters, Milford, MA, USA) coupled with a triple-quadrupole tandem mass spectrometer (Micromass, Waters, Manchester, UK). Chromatographic separations were performed using a SunFire C18 column (3.5  $\mu\text{m}$ , 2.1 mm $\times$ 150 mm, Waters) at an eluent flow rate of 0.2 ml/min using water (eluent A) and acetonitrile (eluent B). Both eluents contained 0.1 % (v/v) formic acid. The eluent compositions were 40:60 (A:B) for PENG and 10:90 (A:B) for CEX. A full scan MS analysis was conducted using electrospray ionization (ESI) in positive ion mode with the following settings: cone voltage = 15 V, capillary voltage = 3000 V, source temperature = 150 °C, desolvation temperature = 350 °C, cone gas flow = 50 L/h, and desolvation gas flow = 500 L/h. The mass spectra of all peaks in the total ion chromatogram (TIC) were obtained using a mass scan range of 100 to 500 m/z. Extracted ion monitoring was performed for masses of expected transformation products (e.g.,

parent molecular structure plus one or two additional oxygen atoms). The CEX samples treated with Fe(VI) were also analysed for ammonia using the phenate method<sup>14</sup>.

*PENG*. Figure S8 shows HPLC/MS chromatograms of a Fe(VI)-treated *PENG* sample ( $[PENG]_0 = 20 \mu\text{M}$  and  $[Fe(VI)]_0 = 40 \mu\text{M}$ ) in a selected ion monitoring mode (SIM) for  $[M+H]^+$  as representative data. A peak with  $m/z$  of 335 was found at a retention time of 6.6 min (Figure S8a). This peak was clearly assigned to *PENG*, which could be confirmed by analyzing a standard solution of *PENG* ( $20 \mu\text{M}$ ). Figure S10 shows the mass spectrum acquired for *PENG*, which is similar to the *PENG* mass spectrum obtained previously using a high-resolution mass spectrometer<sup>13</sup>.

Two peaks with  $m/z$  of 351 were detected at retention times (RTs) of 5.3 and 6.5 min, respectively (Figure S8b). Two peaks with  $m/z$  of 351 were also detected at the same RTs (i.e., 5.3 and 6.5 min) in the ozone-treated *PENG* samples (Figure S9b). These two peaks with a mass of an additional oxygen atom ( $M = 16$ ) compared to *PENG* were assigned to the two stereo-isomeric sulfoxides of *PENG* (i.e., *PENG*-(*R*)- and *PENG*-(*S*)-sulfoxides). The mass spectra of these two peaks (RTs of 5.3 and 6.5 min) are shown in Figure S11 and Figure S12 for the Fe(VI)-treated and ozone-treated samples, respectively. Mass spectra for these peaks were quite consistent for the Fe(VI)- and ozone-treated samples. It was shown previously that the reaction of ozone with *PENG* produced *PENG*-(*R*)-sulfoxide and *PENG*-(*S*)-sulfoxide as the sole primary products<sup>13</sup>. In that study, the order of elution using HPLC with a reverse-phase C16 column was reported as *PENG*-(*R*)-sulfoxide followed by *PENG*-(*S*)-sulfoxide<sup>13</sup>. Based on this, it is concluded that the two peaks with a  $m/z$  of 351 at RTs of 5.3 and 6.5 min in the present study correspond to *PENG*-(*R*)- and *PENG*-(*S*)-sulfoxide, respectively.

A peak with  $m/z$  of 367 was detected at a RT of 12.5 min for the Fe(VI)-treated *PENG* samples. This peak with a mass of additional two oxygen atoms ( $M = 32$ ) compared to *PENG* was assigned to *PENG*-sulfone. The mass spectrum of *PENG*-sulfone is shown in Figure S11c. The peak for *PENG*-sulfone was not found for the ozone-treated *PENG* samples (Figure S9).

During treatment with ozone, the peak areas of *PENG*-(*R*)- and *PENG*-(*S*)-sulfoxides increased for  $[O_3]_0 \leq 20 \mu\text{M}$  and then were stable for  $[O_3]_0 \geq 20 \mu\text{M}$  (Figure S13). This behavior is consistent with a previous study showing that *PENG*-(*R*)- and *PENG*-(*S*)-sulfoxides are the two major and final products from the reaction of ozone with *PENG* under the same conditions<sup>13</sup>. In order to enable estimates of product yields in the Fe(VI) reaction with *PENG*, peak normalizing parameters for *PENG*-(*R*)- and *PENG*-(*S*)-sulfoxides in Figure S13 (i.e.,  $A_{PENG-(R)\text{-sulfoxide},0}$  and

$A_{\text{PENG-(S)-sulfoxide},0}$  were adjusted to satisfy a mass balance based on the peak areas, i.e.,  
 $A_{\text{PENG}}/A_{\text{PENG},0} + A_{\text{PENG-(R)-sulfoxide}}/A_{\text{PENG-(R)-sulfoxide},0} + A_{\text{PENG-(S)-sulfoxide}}/A_{\text{PENG-(S)-sulfoxide},0} = 1$ , and the  
 condition of  $A_{\text{PENG-(R)-sulfoxide},0} = A_{\text{PENG-(S)-sulfoxide},0}$ . This apparent mass balance yielded  $A_{\text{PENG-(R)-sulfoxide},0} = A_{\text{PENG-(S)-sulfoxide},0} = 1.8 \times 10^6$ . Using these values, the molar yields of PENG-(R)- and  
 PENG-(S)-sulfoxides from the reaction of ozone with PENG were determined to be 56% and 44%,  
 respectively, which is consistent with previous results<sup>13</sup>. The obtained  $A_0$  values were then applied  
 to estimate the yields of transformation products in the Fe(VI)-PENG reaction.

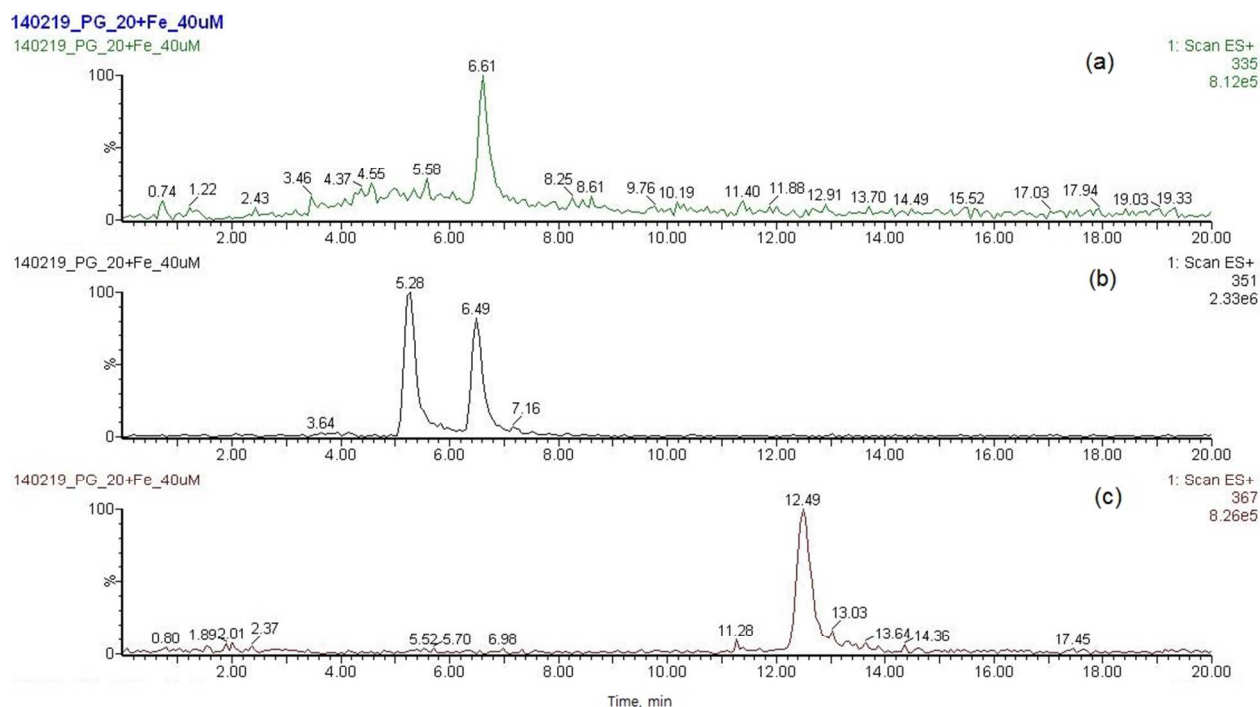


Figure S8. HPLC/MS chromatograms of a Fe(VI)-treated PENG sample in a selected ion monitoring mode (SIM) for  $[M+H^+]$ : (a)  $m/z = 335$ , (b)  $m/z = 351$ , and (c)  $m/z = 367$ . The sample was prepared by reacting 20  $\mu\text{M}$  of PENG with 40  $\mu\text{M}$  of Fe(VI) in 1 mM phosphate buffer at pH 7.

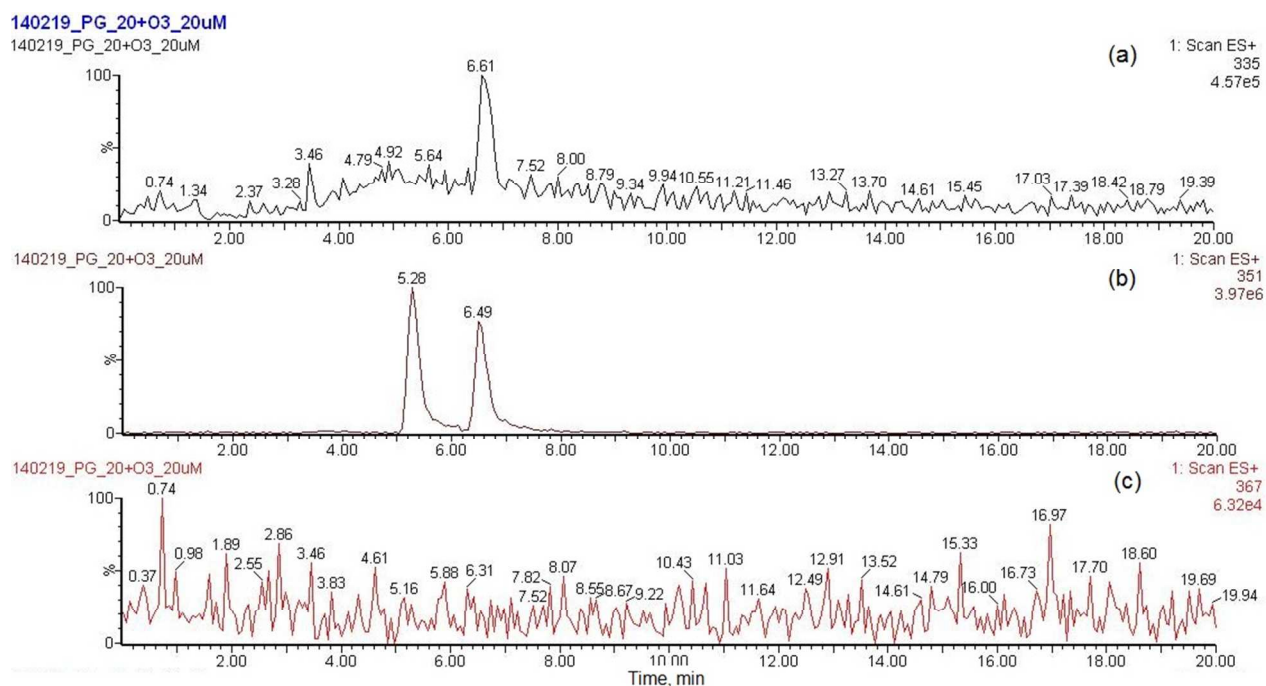


Figure S9. HPLC/MS chromatograms of an ozone-treated PENG sample in a selected ion monitoring mode (SIM) for  $[M+H]^+$ : (a)  $m/z = 335$ , (b)  $m/z = 351$ , and (c)  $m/z = 367$ . The sample was prepared by reacting 20  $\mu$ M of PENG with 20  $\mu$ M of ozone in 1 mM phosphate buffer at pH 7.

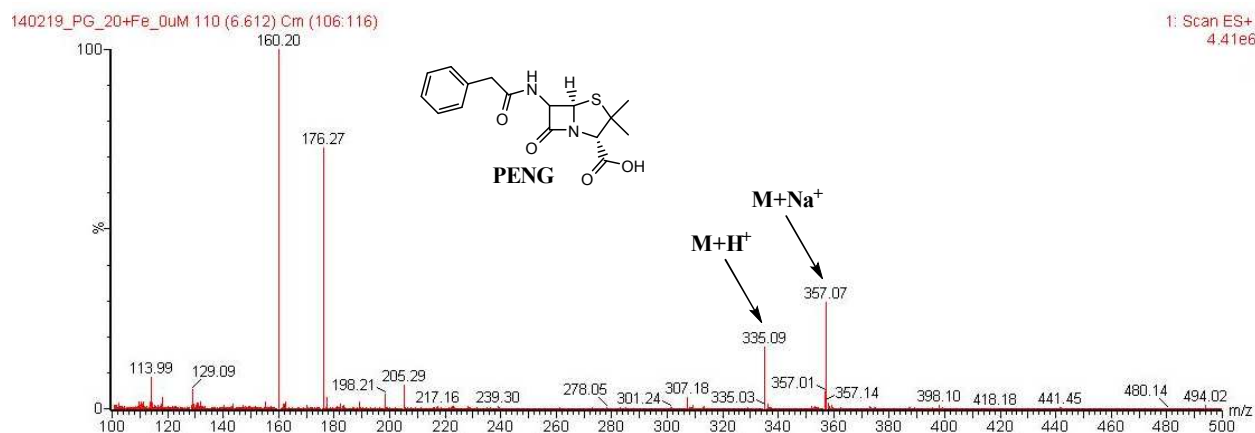


Figure S10. Full-scan, positive-mode ESI mass spectrum acquired for PENG ( $m/z = 335$  and RT = 6.6 min). Mass spectra were obtained using 20  $\mu$ M of PENG.

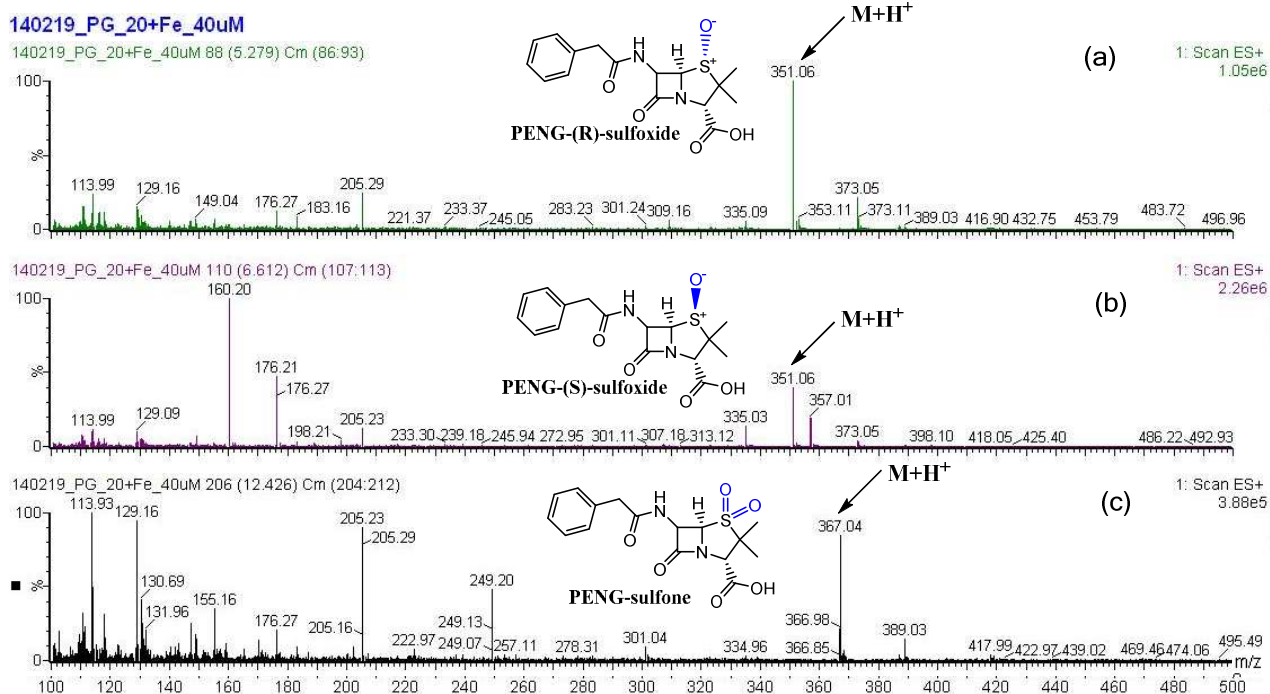


Figure S11. Full-scan, positive-mode ESI mass spectra for (a) PENG-(R)-sulfoxide ( $m/z = 351$  and  $RT = 5.3$  min), (b) PENG-(s)-sulfoxide ( $m/z = 351$  and  $RT = 6.6$  min), and (c) PENG-sulfone ( $m/z = 367.0$  and  $RT = 12.5$  min) acquired from the ferrate(VI)-treated PENG sample ( $[PENG]_0 = 20$   $\mu M$  and  $[Fe(VI)]_0 = 40$   $\mu M$ ).

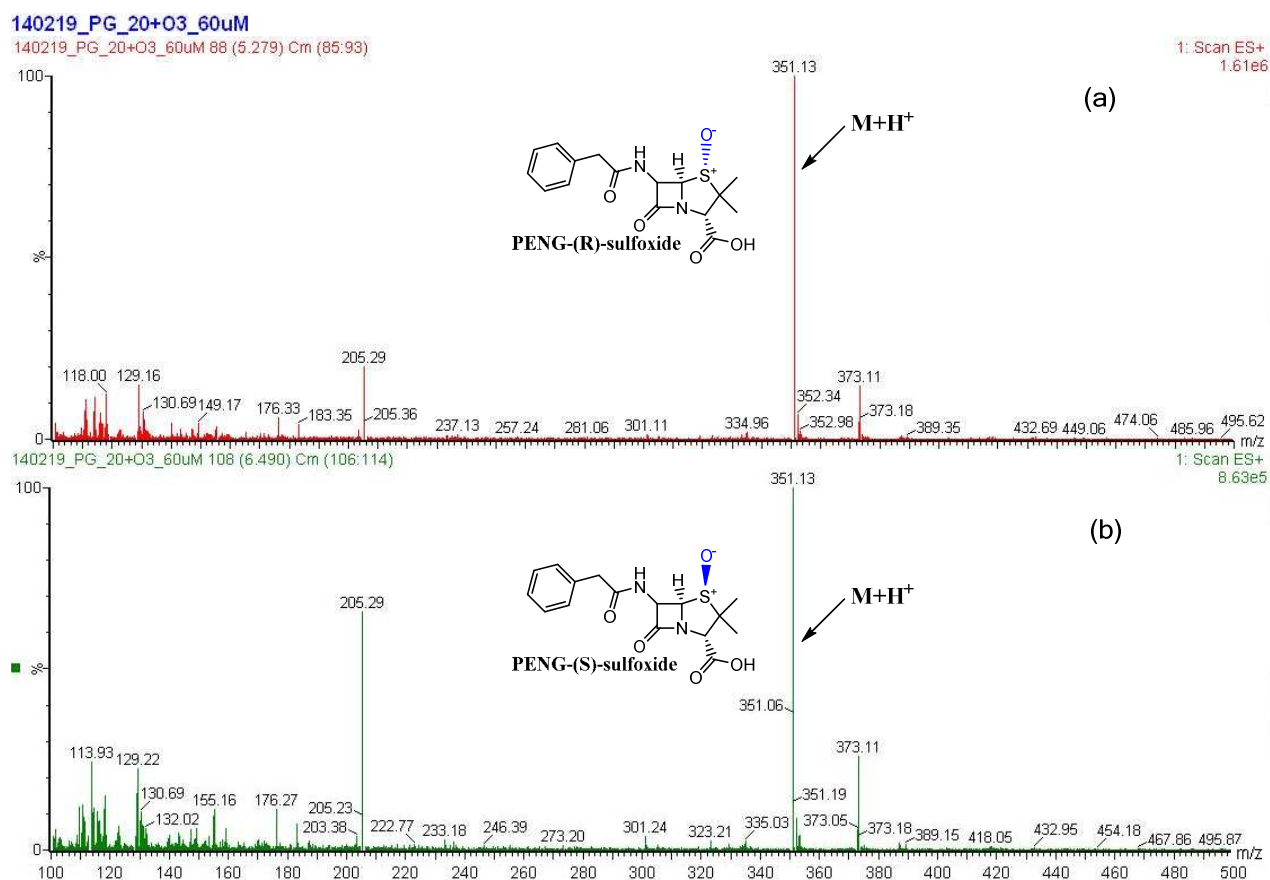


Figure S12. Full-scan, positive-mode ESI mass spectra for (a) PENG-(R)-sulfoxide ( $m/z = 351$  and  $RT = 5.3$  min) and (b) PENG-(s)-sulfoxide ( $m/z = 351$  and  $RT = 6.6$  min) acquired from the ozone-treated PENG sample ( $[PENG]_0 = 20 \mu M$  and  $[O_3]_0 = 60 \mu M$ ). Ozonation was performed in the presence of 10 mM *tert*-butanol as a  $\cdot OH$  radical scavenger.

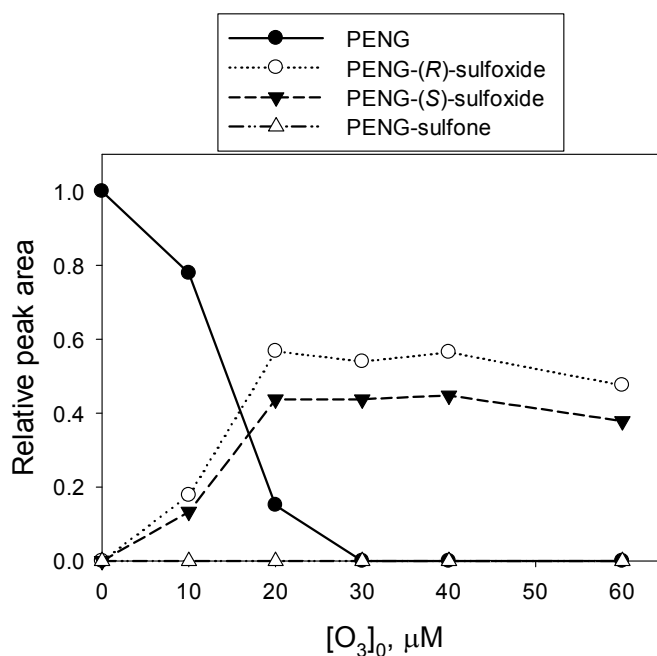
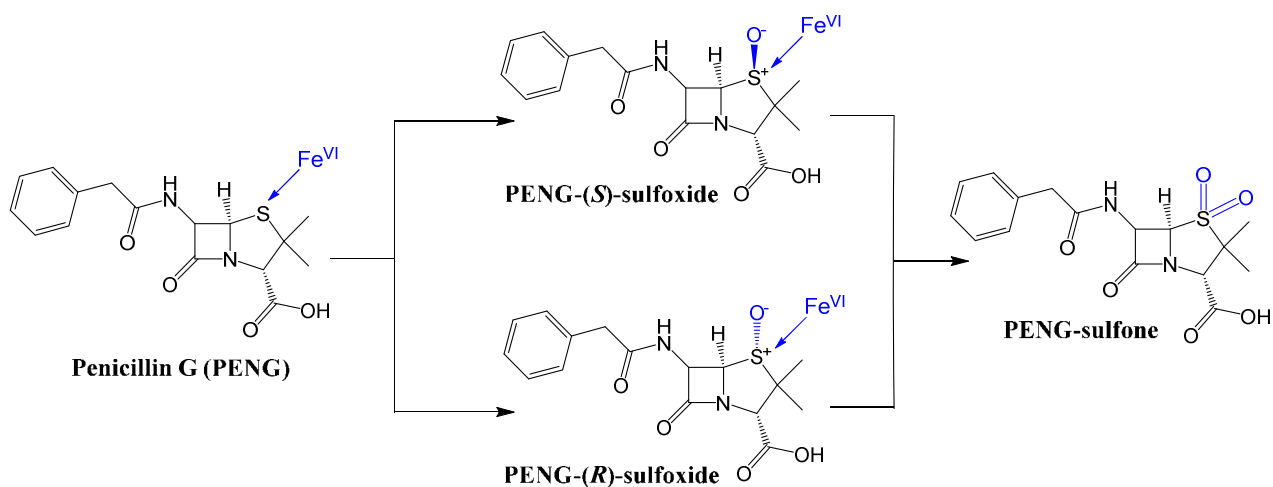


Figure S13. Changes of the relative peak areas ( $A/A_0$ ) for PENG and its transformation products for reactions of PENG ( $[PENG]_0 = 20 \mu M$ ) with ozone ( $[O_3]_0 = 0 - 60 \mu M$ ) at pH 7 (1 mM phosphate buffer). The reaction was conducted in presence of 10 mM *tert*-butanol as a  $\cdot OH$  radical scavenger. Relative peak areas for PENG-(*R*)- and PENG-(*S*)-sulfoxides were adjusted for the ozone-treated samples based on the previous observation that the yields of these products are 55% and 45%, respectively, from the reaction of ozone with PENG<sup>13</sup>. The peak areas of PENG were normalized by the peak area corresponding to PENG at an initial concentration of 20  $\mu M$ .



Scheme S1. Transformation products and reaction pathways for the reaction of  $Fe(VI)$  with penicillin G (PENG).

392

393 *CEX*. Figure S14 shows HPLC/MS chromatograms of a Fe(VI)-treated CEX sample ( $[CEX]_0 =$   
394  $20\ \mu\text{M}$  and  $[\text{Fe(VI)}]_0 = 30\ \mu\text{M}$ ) in selected ion monitoring mode (SIM) for  $[M+H]^+$  as  
395 representative data. A peak with  $m/z$  of 348 was found at a RT of 5.1 min (Figure S14a). This peak  
396 was clearly assigned to CEX, which could be confirmed by analyzing a standard solution of CEX  
397 ( $20\ \mu\text{M}$ ). Figure S16 shows the mass spectrum acquired for CEX.

398 Two peaks with  $m/z$  of 364 were detected at RTs of 2.3 and 2.9 min, respectively (Figure S14b).  
399 Two peaks with  $m/z$  of 364 were also detected at the same RTs (i.e., 2.3 and 2.9 min) in the ozone-  
400 treated CEX samples (Figure S15b). These two peaks with a mass of an additional oxygen atom  
401 ( $M = 16$ ) compared to CEX were assigned to the two stereo-isomeric sulfoxides of CEX (i.e.,  
402 CEX-(*R*)- and CEX-(*S*)-sulfoxides). The mass spectra of these two peaks (RTs of 2.3 and 2.9 min)  
403 are shown in Figure S17 and Figure S18 for the Fe(VI)-treated and ozone-treated samples,  
404 respectively. Mass spectra for these peaks were quite consistent for all samples. It was shown  
405 previously that the reaction of ozone with CEX produced CEX-(*R*)- and CEX-(*S*)-sulfoxide with  
406 yields of 34% and 18%, respectively<sup>13</sup>. In that study, the order of elution using HPLC with a  
407 reverse-phase C16 column was reported as CEX-(*R*)-sulfoxide followed by CEX-(*S*)-sulfoxide<sup>13</sup>.  
408 Therefore, it is concluded that the two peaks at RTs of 2.3 and 2.9 min in the present study are  
409 CEX-(*R*)- and CEX-(*S*)-sulfoxide, respectively.

410 A peak with  $m/z$  of 380 was detected at a RT of 3.2 min for the ferrate(VI)-treated CEX  
411 samples (Figure S14c). This peak with a mass of additional two oxygen atoms ( $M = 32$ ) compared  
412 to CEX was assigned to CEX-sulfone. The mass spectrum of CEX-sulfone is shown in Figure  
413 S17c. The peak for CEX-sulfone was not found for the ozone-treated CEX samples (Figure S15c).  
414 This is consistent with the case of PENG, in which PENG-sulfone is not formed upon ozonation  
415 (see above).

416 A peak with  $m/z$  of 398 was detected at a RT of 5.7 min for the ozone-treated CEX samples  
417 (Figure S15d). A product with  $m/z$  of 398 was also found previously, and identified as having  
418 undergone ozonolysis at the olefin-moiety<sup>13</sup>. For the Fe(VI) reactions, transformation products  
419 with a cleaved olefin-moiety are not expected, especially for low Fe(VI) exposure, due to the low  
420 reactivity of the olefin moiety to Fe(VI) (i.e.,  $k_{\text{app}} = 2.3\ \text{M}^{-1}\ \text{s}^{-1}$  for MCA at pH 7; see Table S1).

421 Figure S19 shows the changes of relative peak areas ( $A/A_0$ ) for CEX and its transformation  
422 products for reactions of  $20\ \mu\text{M}$  CEX at a range of initial ozone concentrations. The peak areas of  
423 CEX-(*R*)- and CEX-(*S*)-sulfoxide increased and then decreased with increasing initial ozone



concentration, indicating that these products are formed from the attack of ozone at the thioether moiety of CEX and then transformed further. The peak area corresponding to the product with  $m/z$  of 398 (i.e., CEX-P398) also increased and then decreased with increasing initial ozone concentration, indicating that this product is formed from the attack of ozone at the olefin-moiety of CEX and then transformed further. These observations are consistent with prior work<sup>13</sup>. Peak area normalizing parameters ( $A_0$ ) for CEX-(*R*)- and CEX-(*S*)-sulfoxide were determined in the same manner as for the PENG-sulfoxides, based on previously reported yields of these two products in reaction of CEX with ozone under the same conditions (i.e., 34% and 18%, respectively)<sup>13</sup>. The obtained  $A_0$  values were then applied to estimate the yields of transformation products in the Fe(VI)-CEX reaction.

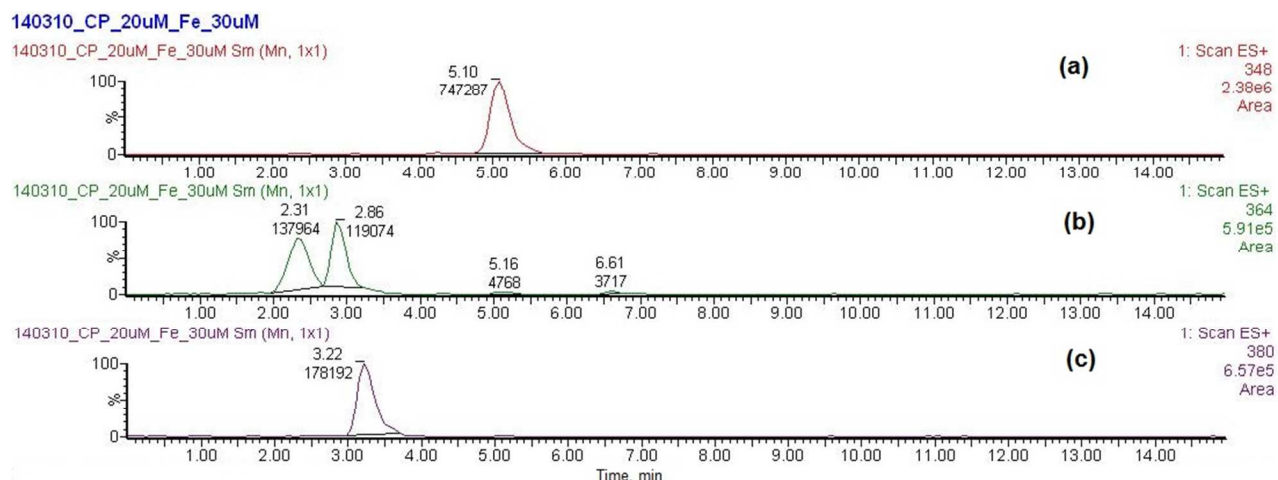


Figure S14. HPLC/MS chromatograms of a ferrate(VI)-treated CEX sample in a selected ion monitoring mode (SIM) for  $[M+H]^+$ : (a)  $m/z = 348$ , (b)  $m/z = 364$ , and (c)  $m/z = 380$ . The sample was prepared by reacting 30  $\mu\text{M}$  of Fe(VI) with 20  $\mu\text{M}$  of CEX in 1 mM phosphate buffer at pH 7.

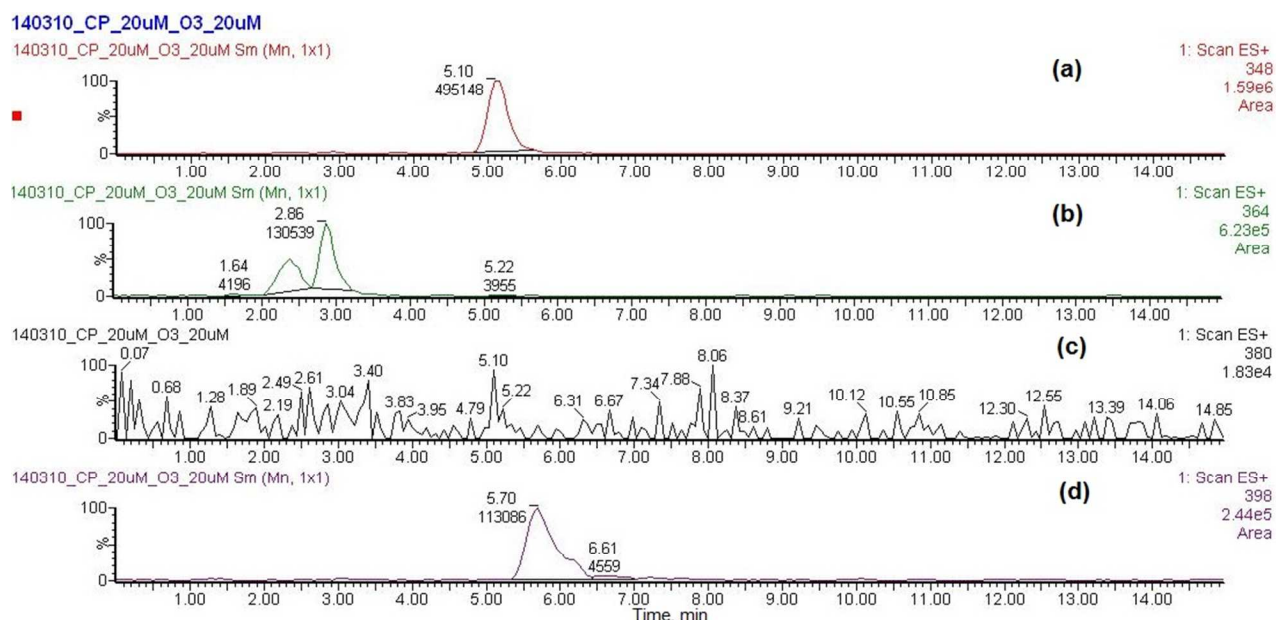


Figure S15. HPLC/MS chromatograms of an ozone-treated CEX sample in a selected ion monitoring mode (SIM) for  $[M+H]^+$ : (a)  $m/z = 348$ , (b)  $m/z = 364$ , (c)  $m/z = 380$ , and (d)  $m/z = 398$ . The sample was prepared by reacting 20  $\mu\text{M}$  of ozone with 20  $\mu\text{M}$  of CEX in 1 mM phosphate buffer at pH 7.

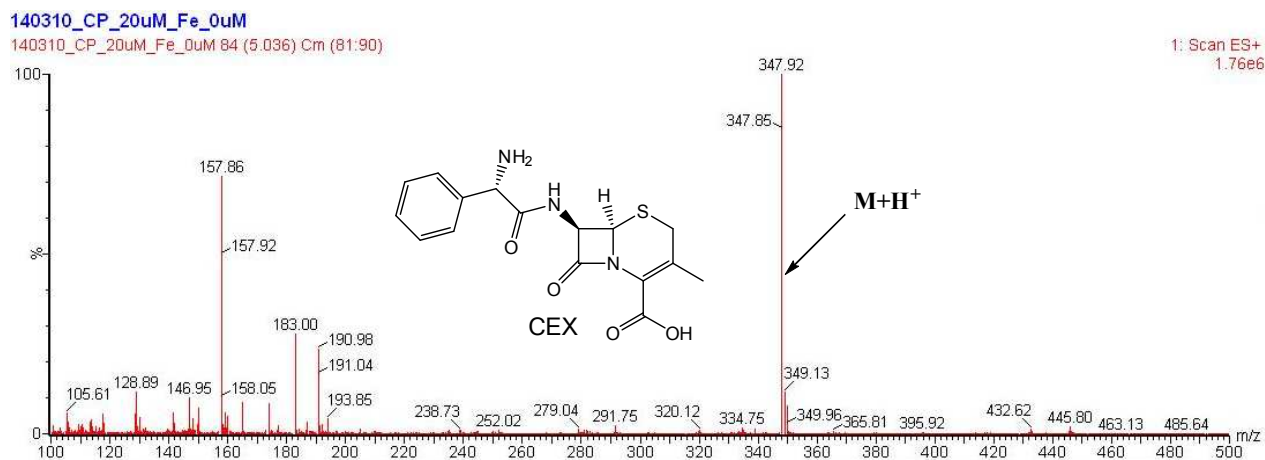


Figure S16. Full-scan, positive-mode ESI mass spectrum acquired for CEX ( $m/z = 348$  and RT = 5.0 min). Mass spectra were obtained using 20  $\mu\text{M}$  of CEX.

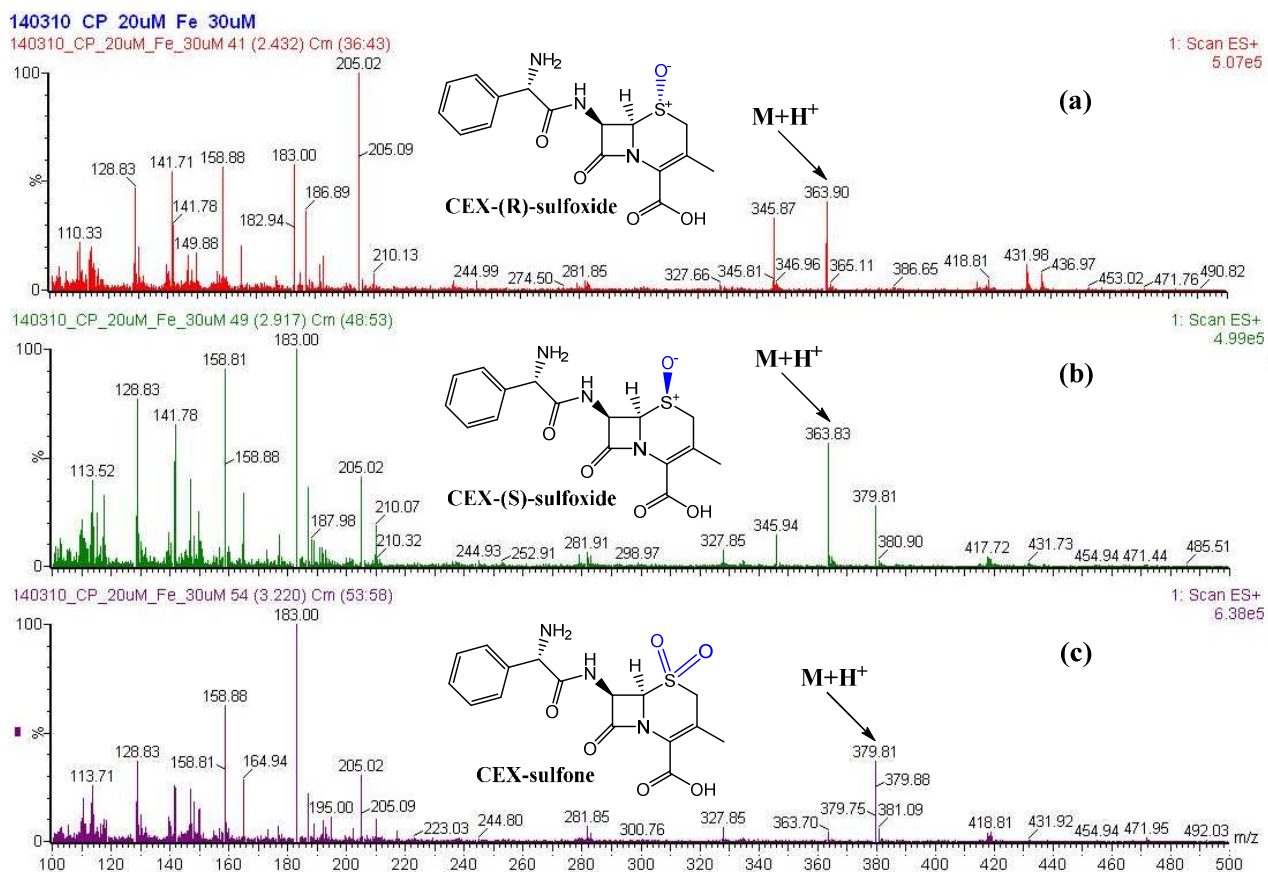
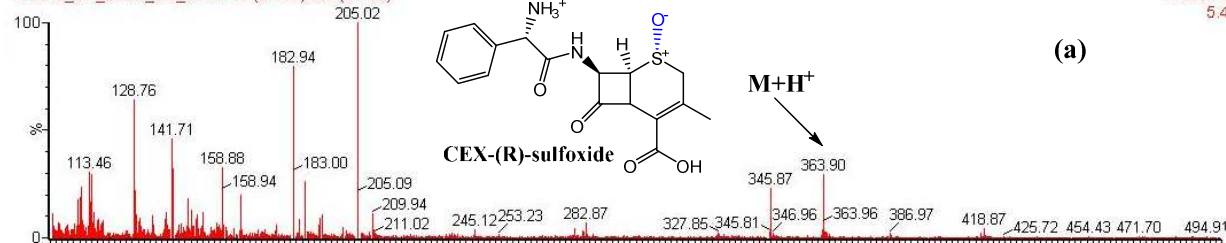


Figure S17. Full-scan, positive-mode ESI mass spectra for (a) CEX-(R)-sulfoxide ( $m/z$  = 364 and RT = 2.4 min), (b) CEX-(s)-sulfoxide ( $m/z$  = 364 and RT = 2.9 min), and (c) CEX-sulfone ( $m/z$  = 380 and RT = 3.2 min) acquired from the ferrate(VI)-treated CEX sample ( $[CEX]_0 = 20 \mu M$  and  $[Fe(VI)]_0 = 30 \mu M$ ).

140310\_CP\_20uM\_O3\_20uM

140310\_CP\_20uM\_O3\_20uM 42 (2.493) Cm (37.43)

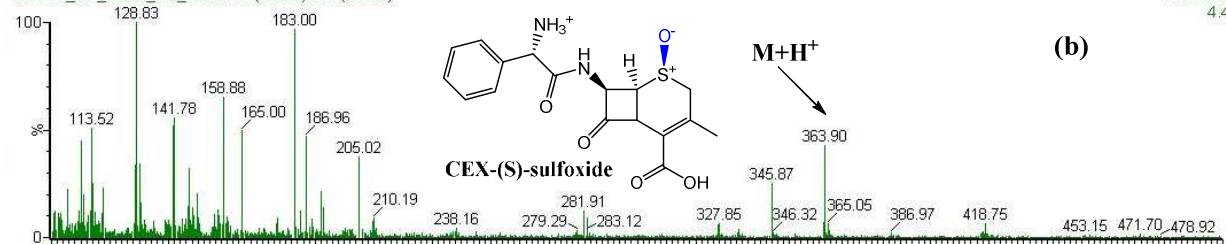
1: Scan ES+  
5.44e5



(a)

140310\_CP\_20uM\_O3\_20uM 48 (2.856) Cm (48.52)

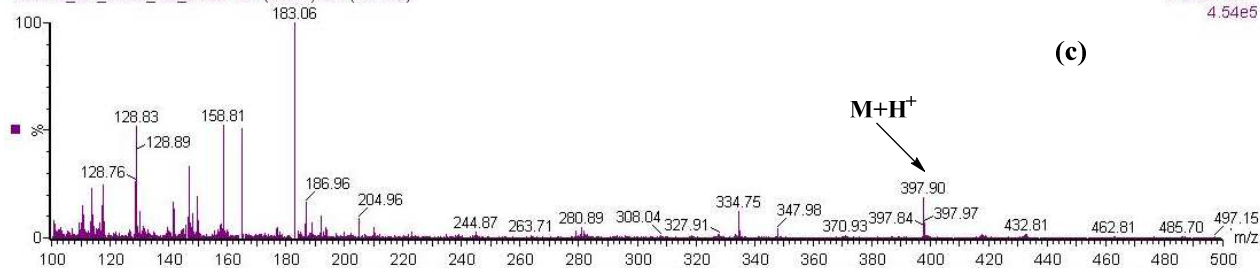
1: Scan ES+  
4.48e5



(b)

140310\_CP\_20uM\_O3\_20uM 101 (6.066) Cm (92.102)

1: Scan ES+  
4.54e5



(c)

Figure S18. Full-scan, positive-mode ESI mass spectra for (a) CEX-(R)-sulfoxide ( $m/z = 364$  and  $RT = 2.3$  min), (b) CEX-(s)-sulfoxide ( $m/z = 364$  and  $RT = 2.8$  min), and (c) CEX-P398 ( $m/z = 398$  and  $RT = 5.7$  min) acquired from the ozone-treated CEX sample ( $[CEX]_0 = 20 \mu M$  and  $[O_3]_0 = 20 \mu M$ ).

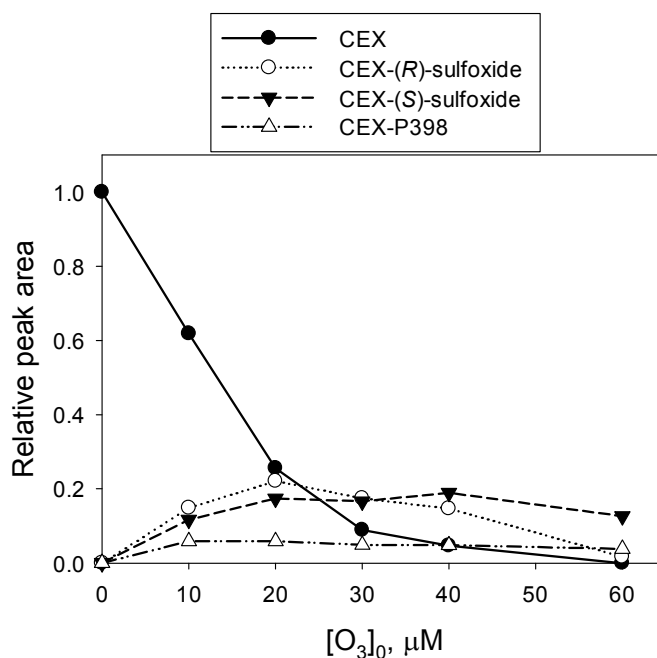
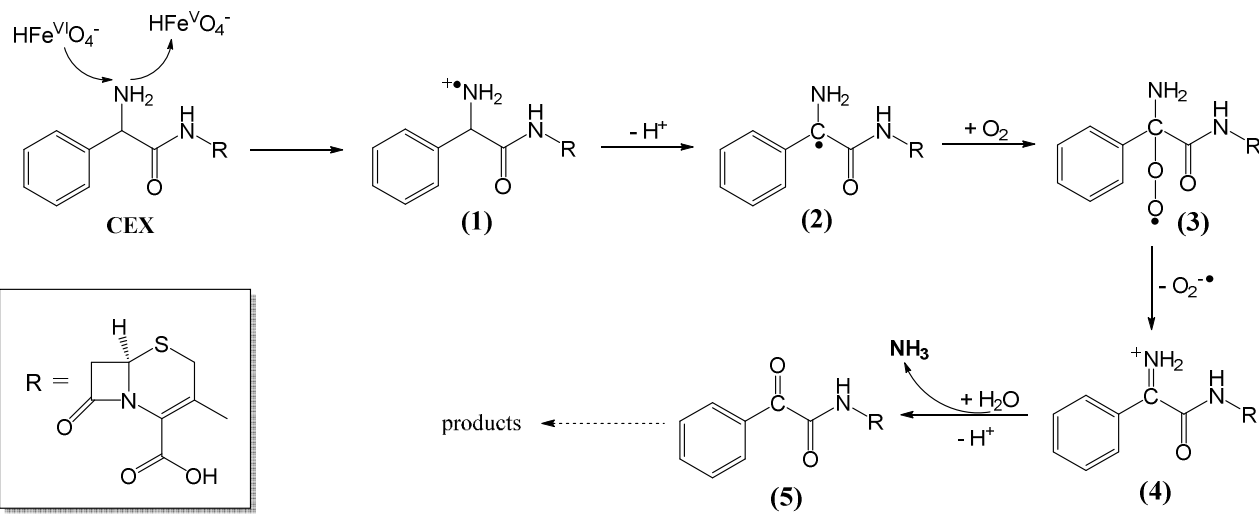


Figure S19. Changes of the relative peak areas ( $A/A_0$ ) or relative concentrations ( $C/C_0$ ) for CEX and its transformation products for reactions of CEX ( $[CEX]_0 = 20 \mu\text{M}$ ) with ozone ( $[O_3]_0 = 0 - 60 \mu\text{M}$ ) at pH 7 (1 mM phosphate buffer). The reaction was conducted in the presence of 10 mM *tert*-butanol as a  $\cdot\text{OH}$  radical scavenger. Relative peak areas for CEX-(*R*)- and CEX-(*S*)-sulfoxides for the ozone-treated samples were adjusted based on the previous observation that the initial yields of these two products were 34% and 18%, respectively, from the reaction of ozone with CEX<sup>13</sup>. The peak areas of CEX and CEX-P398 were normalized by the peak area corresponding to CEX at an initial concentration of 20  $\mu\text{M}$ .



Scheme S2. Proposed reaction mechanisms for the oxidation of the amine-moiety of CEX by ferrate(VI). One-electron oxidation of the primary amine of CEX forms an aminium radical cation (1) that subsequently deprotonates into the neighboring C-centered radical (2). In the presence of oxygen, the C-centered radical (2) react rapidly with oxygen and generates an iminium cation (4) and superoxide radical ( $\text{O}_2^{\bullet -}$ ) via a peroxy radical intermediate (3). The iminium cation (4) hydrolyzes into a di-acetyl compound (5) and ammonia.

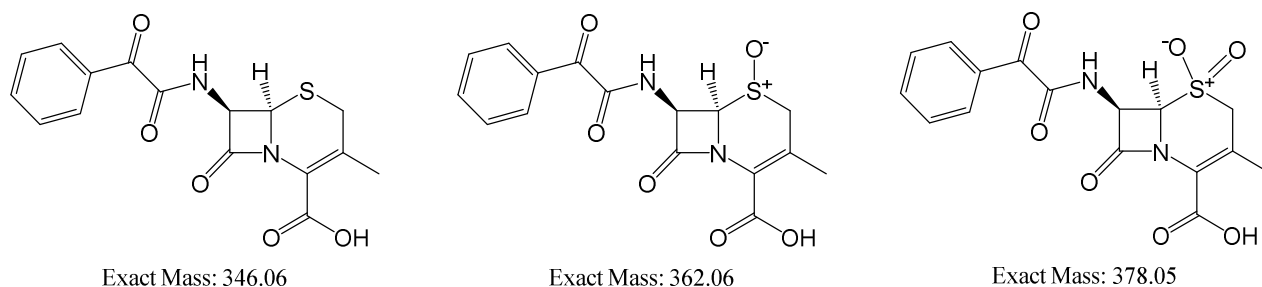
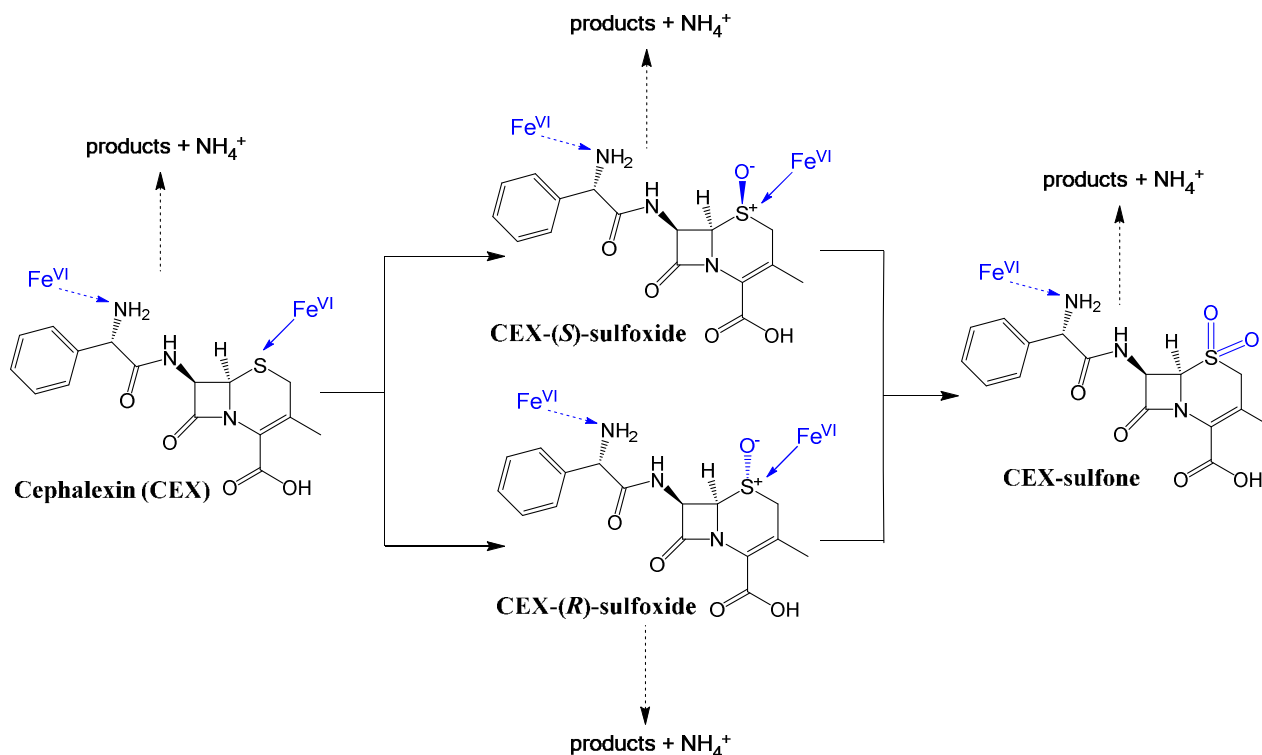


Figure S20. Probable amine-transformation products of CEX with the di-acetyl moiety. None of these potential intermediate products were detected in the HPLC/MS analysis (in either positive- or negative-mode full-scan). They could have been further transformed into hydrolyzed products or escaped from the mass detection due to low sensitivity.



Scheme S3. Transformation products and reaction pathways for the reaction of Fe(VI) with cephalixin (CEX).

*Transformation pathways of the other  $\beta$ -lactams.* In light of the similar structures and reactivity of CLOX and PENG toward Fe(VI) (Table S1), the transformation pathway of CLOX is anticipated to be comparable to that of PENG (Scheme S1). For AMP and AMX, the amine moiety is the primary reaction site followed by the thioether moiety (AMP) or thioether and phenol moieties (AMX) (Figure 1). The transformation pathways of these two compounds can thus be predicted to some degree based on the kinetic information provided in Figure 1 and Table S1 and the reaction pathways elucidated here for PENG and CEX. Further research is needed to characterize the transformation products resulting from reaction of Fe(VI) with the AMX phenol group.

#### **SI-Text-9. Measurement of antibacterial activities after treatment of $\beta$ -lactams with ferrate(VI) (adapted from Dodd et al., 2009<sup>15</sup>)**

*Broth microdilution assay.* For quantitative antibacterial activity measurements, this study employed the broth microdilution assay developed by Dodd et al.<sup>15</sup>, which is based on cell growth inhibition. Here, a brief description of the method is provided. Samples were prepared by reacting 10  $\mu$ M of each  $\beta$ -lactam (PENG, CLOX, AMX, and CEX) with a range of Fe(VI) dose (0 – 60  $\mu$ M) at pH 7 (1 mM phosphate buffer). After complete Fe(VI) consumption ( $\geq 3$  hrs), each Fe(VI)-treated sample was used to prepare ten-member dilution series via 1:1 serial dilution using 1 mM phosphate buffer of pH 7. The same dilution series were also prepared for untreated samples (i.e., initial  $\beta$ -lactam samples). 100  $\mu$ L of ten-member dilution series from each sample were located in wells in a row of a 96-well microtiter plate. These samples prepared in a 96-well microtiter plate were then inoculated with 100  $\mu$ L of Mueller-Hinton broth containing  $1 \times 10^6$  CFU/mL of the reference *B. subtilis* strains (KCCM, 11316). Working *B. subtilis* stock cultures were maintained at 30 °C on nutrient agar. Broth cultures were prepared by suspending *B. subtilis* cells sampled from the working cultures in 5 mL of Mueller-Hinton broth in polypropylene test tubes and incubated overnight at 30 °C in a shaker rotating at 200 rpm. The prepared plates were then sealed with breathable Rayon sealing tape (Thermo Scientific, NUNC 241205) to minimize evaporative water loss and incubated at 30 °C for ~8 h with 200 rpm agitation. After incubation, the sealing tape was

removed and the plates were re-sealed with impermeable polyester sealing tape (Thermo Scientific, NUNC 236370) and agitated vigorously using a Vortex microtiter plate shaker to re-suspend the cells in the wells. The polyester tape was then removed and the absorbance of the solutions in each well was measured at 625 nm as a surrogate for cell density using a FLx800<sup>TM</sup> microplate reader (BioTek, USA).

*Analysis of dose-response data.* The absorbance measurements,  $A$  (at 625 nm), obtained by the microplate reader were converted to growth inhibition,  $I$  (in %), by scaling them to the absorbance measurements  $A_{\min}$  (corresponding to 100% growth inhibition) and  $A_{\max}$  (corresponding to 0% growth inhibition), via eq S8.

$$I(\%) = \frac{(A_{\max} - A)}{(A_{\max} - A_{\min})} \times 100 \quad (\text{S8})$$

In the previous broth microdilution assay proposed by Dodd et al<sup>15</sup>,  $A_{\max}$  and  $A_{\min}$  values were obtained from separate positive (i.e., cell growth in absence of  $\beta$ -lactam) and negative growth control wells (i.e.,  $\beta$ -lactam in absence of cells), respectively. In the present study, however, the  $A$  values from positive or negative controls were sometimes significantly different from the maximum or minimum  $A$  values of the dose-response curves obtained from each plate. Reasons for such difference are not clear. Therefore, the following alternative method was used in this study.  $A_{\max}$  values were obtained by averaging several maximum  $A$  values of dose-response curves in each plate (usually observed for the most diluted samples). Similarly,  $A_{\min}$  values were obtained by averaging the several minimum  $A$  values in each plate (usually observed for the least diluted samples).

The  $I$  values obtained for each sample dilution series were then plotted against the log of the corresponding sample dilution ( $1/2^n$ ), where  $n$  represents the number of the dilution step. This generates dose-response relationships from which quantitative measures of potency could be extracted. Each dose-response relationship was then fitted to eq S9, a four-parameter logistic regression model.

$$I(\%) = I_{\min} + \frac{(I_{\max} - I_{\min})}{(1 + 10^{(\log(\text{EC}_{50}/(\frac{1}{2^n})) \times H))}} \quad (\text{S9})$$

where  $I_{\max}$  and  $I_{\min}$  represent the maximum and minimum growth inhibition values for a given data set,  $\text{EC}_{50}$  represents the effective concentration (or sample dilution factor in this study) at which 50% growth inhibition is observed,  $n$  is the number of dilution step (i.e.,  $n=1,2,\dots,10$ ), and  $H$  represents the Hill slope, respectively.



The ‘EC50 Shift’ option in the GraphPad Prism software (<http://www.graphpad.com/scientific-software/prism/>) was used to fit simultaneously all dose-response data from each plate using the eq S3 with the constraints of the shared values of  $H$ ,  $I_{\max}$  and  $I_{\min}$  while allowing  $\log(\text{EC}_{50})$  to vary. The antibacterial activity of samples, which is expressed as a ‘potency equivalent’ (PEQ) value, was calculated as the ratio of the  $\text{EC}_{50}$  of the untreated  $\beta$ -lactam (10  $\mu\text{M}$ ) to the  $\text{EC}_{50}$  of each treated sample, i.e.,  $\text{PEQ} = \text{EC}_{50}(\beta\text{-lactam})/\text{EC}_{50}(\text{sample})$ . 95% confidence limits of the  $\log(\text{EC}_{50})$  values calculated by the Prism software were used to determine the 95% confidence limits of the corresponding PEQs. Figure S21 shows an example plot of (a) dose-response relationships for PENG samples treated with increasing Fe(VI) dose and (b) a corresponding plot of the stoichiometry with which PENG is deactivated by Fe(VI).

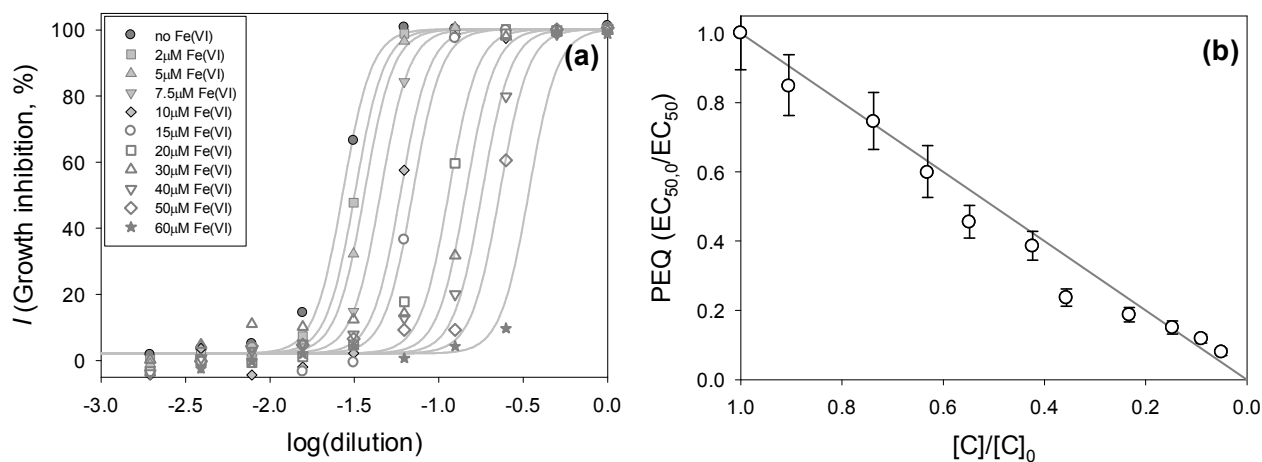


Figure S21. Example plot of (a) dose-response relationships for PENG samples treated with increasing Fe(VI) dose and (b) a corresponding plot of the stoichiometry with which PENG is deactivated by Fe(VI). The error bars represent 95% confidence limits.

*Estimation of antibacterial activity of transformation products.* The theoretical antibacterial activity of samples, PEQ, can be calculated by adding up all the relative concentration of chemicals (i.e., parent  $\beta$ -lactam and its transformation products) multiplied with the corresponding relative antibacterial potency ( $\text{RP}_i$ ) as shown in eq S10.

$$\text{PEQ} = \text{RP}_{\text{parent}} \cdot [\text{C}]/[\text{C}]_0 + \sum_i \text{RP}_i \cdot [\text{TP}]_i/[\text{C}]_0 \quad (\text{S10})$$

By taking  $RP_{parent} = 1$  (definition) and by introducing  $RP_{i,ave}$  as a relative average antibacterial potency of the transformation products (i.e.,  $RP_{i,ave} = \frac{\sum_i RP_i \cdot [TP]_i / [C]_0}{\sum_i [TP]_i / [C]_0}$ ), eq S11 can be derived from the eq S10.

$$PEQ = [C]/[C]_0 + RP_{i,ave} \sum_i [TP]_i / [C]_0 \quad (S11)$$

Finally, eq S12 could be derived by rearranging the eq S11, and was used to estimate the average antibacterial potency ( $RP_{i,ave}$ ) of the transformation products observed during treatment of each  $\beta$ -lactam with Fe(VI).

$$RP_{i,ave} = \frac{PEQ - [C]/[C]_0}{\sum_i [TP]_i / [C]_0} = \frac{PEQ - [C]/[C]_0}{([C]_0 - [C])/[C]_0} \quad (S12)$$

The average antibacterial potencies of the transformation products were obtained by evaluating the PEQ vs.  $[C]/[C]_0$  plot at more than 80% transformation of the parent (i.e.,  $[C]/[C]_0 < 0.2$ ). The results were 5( $\pm$ 3)% for PENG, 0( $\pm$ 3)% for CLOX, -2( $\pm$ 2)% for AMOX, and 26( $\pm$ 11)% for CEX, respectively.

## References

- (1) Bielski, B.H.J.; Thomas, M.J. Studies of hypervalent iron in aqueous solutions. 1. Radiation-induced reductions of iron(VI) to iron(V) by  $CO_2^-$ . *J. Am. Chem. Soc.* **1987**, *109*, 7761–7764.
- (2) Lee, Y.; Yoon, J.; von Gunten, U. Spectrophotometric determination of ferrate (Fe(VI)) in water by ABTS. *Wat. Res.* **2005**, *39*, 1946–1953.
- (3) Huber, M.M.; Canonica, S.; Park, G.Y.; von Gunten, U. Oxidation of pharmaceuticals during ozonation and advanced oxidation processes. *Environ. Sci. Technol.* **2003**, *37*, 1016–1024.
- (4) Lee, Y.; Zimmermann, S. G.; Kieu, A. T.; von Gunten, U. Ferrate (Fe(VI)) application for municipal wastewater treatment: A novel process for simultaneous micropollutant oxidation and phosphate removal. *Environ. Sci. Technol.* **2009**, *43*, 3831–3838.
- (5) Lee, Y.; Kissner, R.; von Gunten, U. Reaction of ferrate(VI) with ABTS and self-decay of ferrate(VI): kinetics and mechanisms. *Environ. Sci. Technol.* **2014**, *48*, 5154–5162.
- (6) Thompson, J.E. *A practical guide to contemporary pharmacy practice*; Lippincott Williams & Wilkins, Philadelphia, 1998.

- 606 (7) Johnson, M.D.; Read, J.F. Kinetics and mechanism of the ferrate oxidation of thiosulfate and  
607 other sulfur-containing species. *Inorg. Chem.* **1996**, *35*, 6795–6799.
- 608 (8) Read, J.F.; MacCormick, K.J.; McBain, A.M. The kinetics and mechanism of the oxidation of  
609 DL ethionine and thiourea by potassium ferrate. *Trans. Met. Chem.* **2004**, *29*, 149–158.
- 610 (9) Read, J.F.; Boucher, K.D.; Mehlman, S.A.; Watson, K.J. The kinetics and mechanism of the  
611 oxidation of 1,4-thioxane by potassium ferrate. *Inorg. Chim. Acta* **1998**, *267*, 159–163.
- 612 (10) Deborde, M.; von Gunten, U. Reactions of chlorine with inorganic and organic compounds  
613 during water treatment-kinetics and mechanisms: a critical review. *Water Res.* **2008**, *42*, 13–51.
- 614 (11) Sharma, V.K.; Liu, F.; Tolan, S.; Shon, M.; Kim, H.; Oturan, M.A. Oxidation of  $\beta$ -lactam  
615 antibiotics by ferrate(VI). *Chem. Eng. J.* **2013**, *221*, 446–451.
- 616 (12) Anquandah, G.A.K.; Sharma, V. K.; Panditi, V.R.; Gardinali, P.R.; Kim, H.; Oturan, M.A.  
617 Ferrate(VI) oxidation of propranolol: kinetics and products. *Chemosphere* **2013**, *91*, 105–109.
- 618 (13) Dodd, M.C.; Rentsch, D.; Singer, H.P.; Kohler, H.E.; von Gunten, U. Transformation of  $\beta$ -  
619 lactam antibacterial agents during aqueous ozonation: reaction pathways and quantitative  
620 bioassay of biologically-active oxidation products. *Environ. Sci. Technol.* **2010**, *44*,  
621 5940–5948.
- 622 (14) American Public Health Association (APHA). *Standard Methods for the Examination of*  
623 *Water and Wastewater*, 20th ed.; APAH: Washington, DC, 1998.
- 624 (15) Dodd, M.C.; Kohler, H.E.; von Gunten, U. Oxidation of antibacterial compounds by ozone  
625 and hydroxyl radical: elimination of biological activity during aqueous ozonation processes.  
626 *Environ. Sci. Technol.* **2009**, *43*, 2498–2504.